e30 Atlas of Neuroimaging

Andre Furtado, William P. Dillon

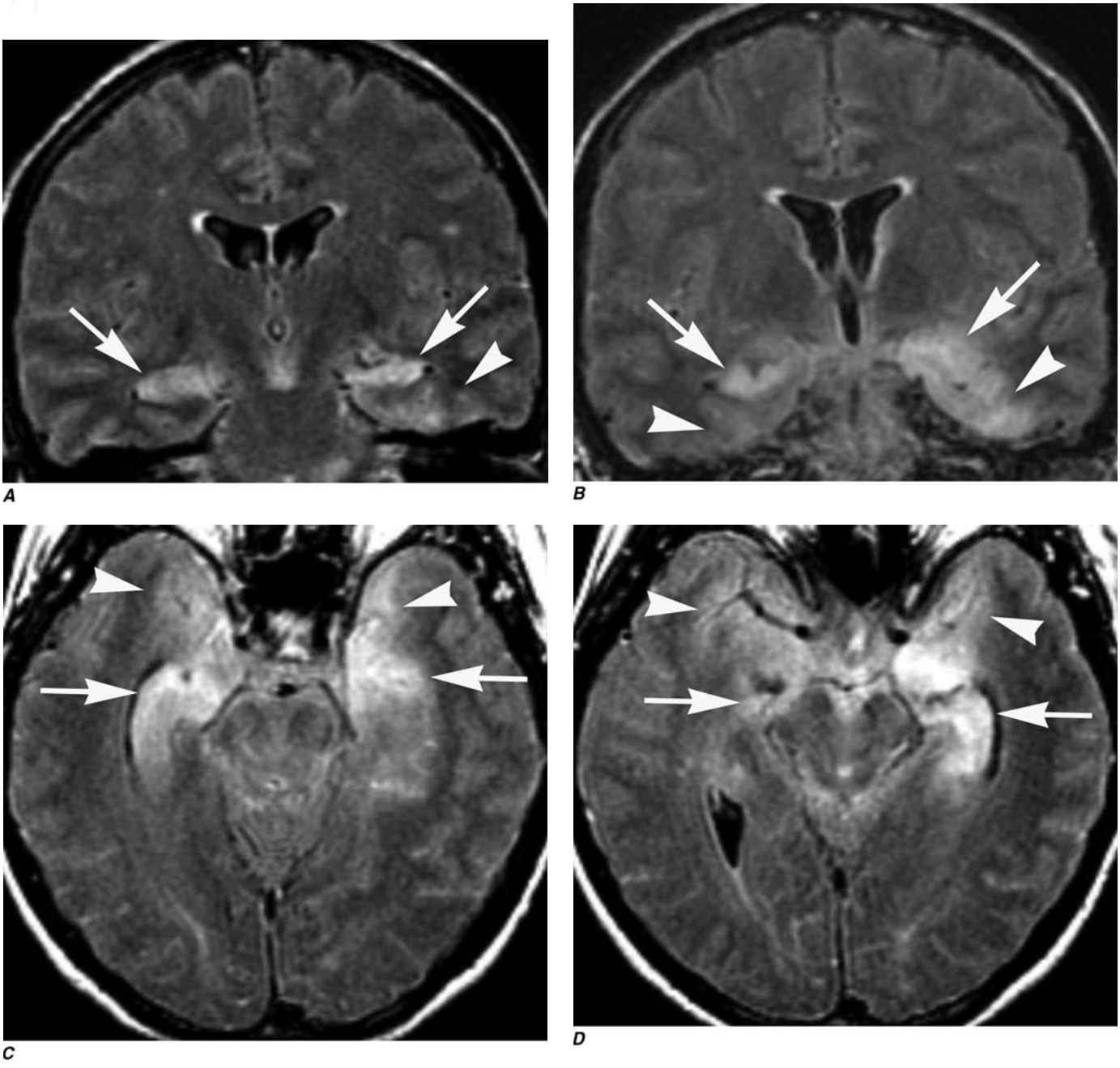

FIGURE e30-1 Limbic encephalitis (Chap. 97)
Coronal (***A***, ***B***), axial FLAIR (***C***, ***D***), and axial T2-weighted (***E***) MR images demonstrate abnormal high signal involving the bilateral mesial temporal lobes (*arrowheads*) including the hippocampi (left greater than right) without significant mass effect (*arrows*). There was no enhancement on post-gadolinium images (not shown). *(continued)*

Copyright © 2008 The McGraw-Hill Companies. All rights reserved.

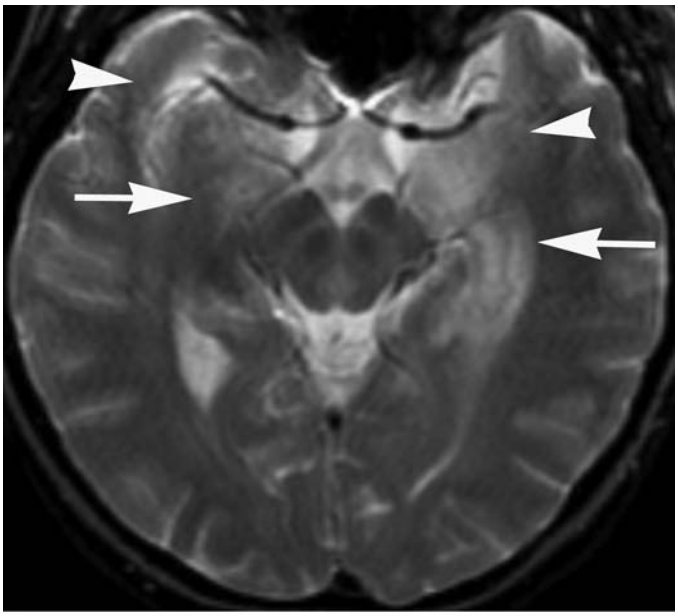

E

FIGURE e30-1 (*Continued*)

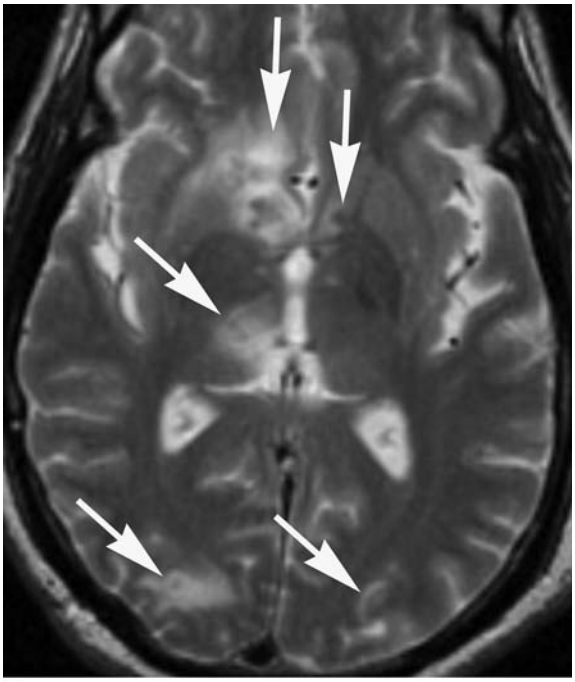

A

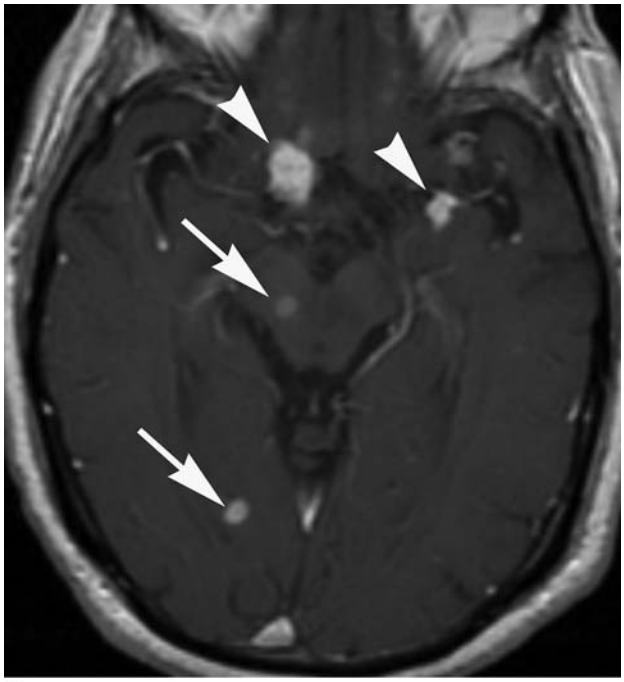

B

FIGURE e30-2 **CNS tuberculosis** (Chap. 158)
Axial T2-weighted MRI (***A***) demonstrates multiple lesions (*arrows*) with peripheral high signal and central low signal, located predominantly in the cortex and subcortical white matter, as well as in the basal ganglia. Axial T1-weighted MR images post-gadolinium (***B***, ***C***) demonstrate ring enhancement of the lesions (*arrows*) and additional lesions in the subarachnoid space (*arrowheads*). *(continued)*

Copyright © 2008 The McGraw-Hill Companies. All rights reserved.

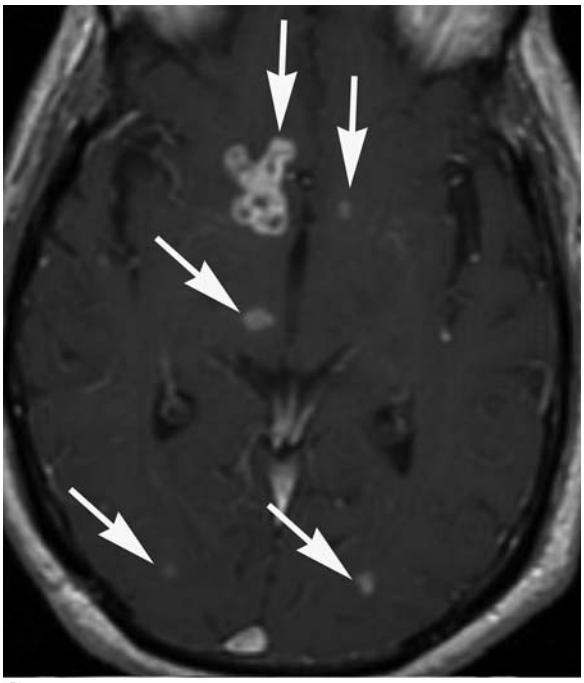

C

D

E

FIGURE e30-2 (*Continued*)
Sagittal T2-weighted MR image of the cervical spine (***D***) demonstrates a hypointense lesion in the subarachnoid space at the level of T5 (*arrow*).
Sagittal T1-weighted MR image post-gadolinium of the cervical spine (***E***) demonstrates enhancement of the lesion in the subarachnoid space at the level of T5 (*arrow*).

Copyright © 2008 The McGraw-Hill Companies. All rights reserved.

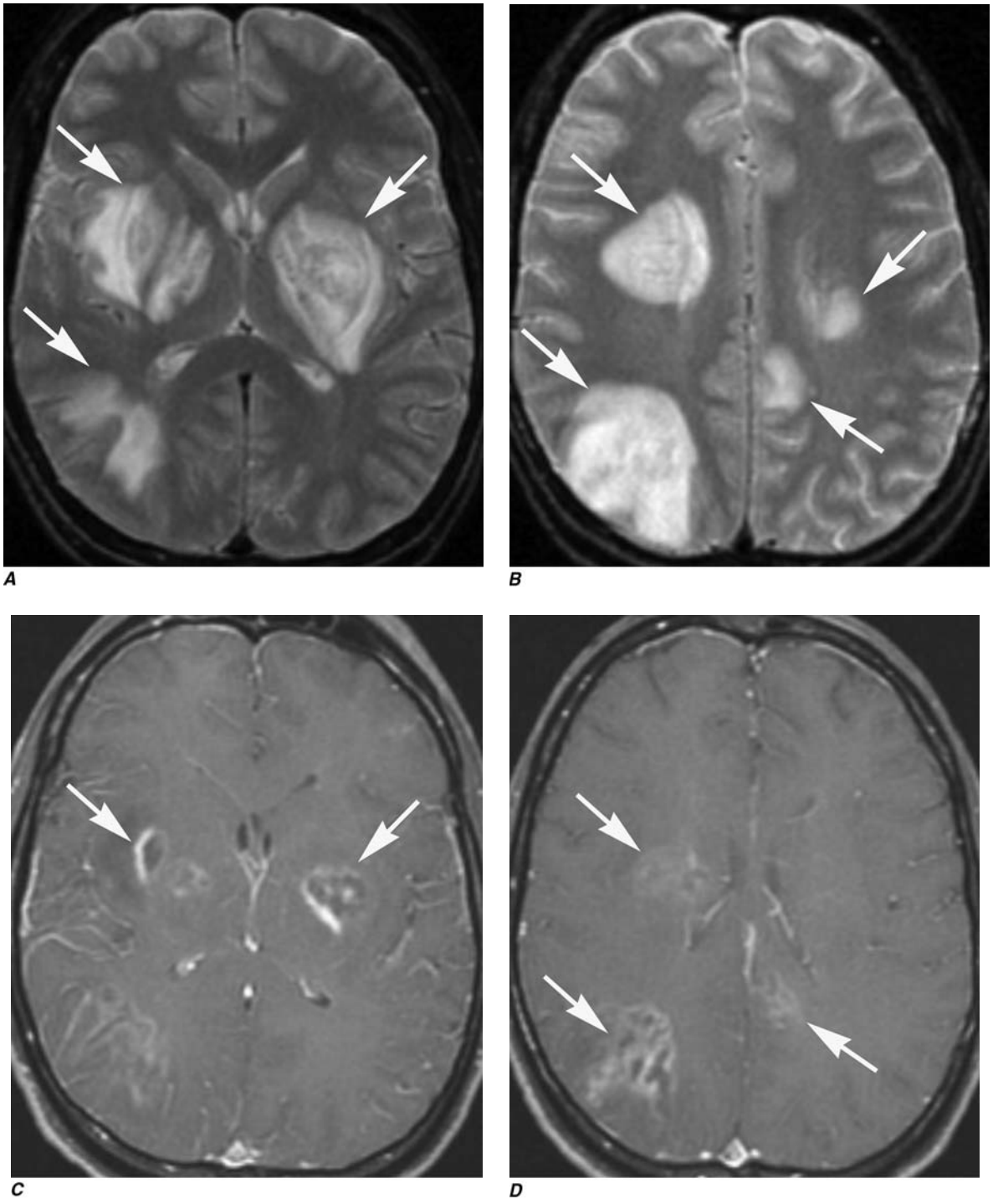

FIGURE e30-3 Neurosyphilis (Chap. 162)
Case I
Axial T2-weighted MR images (***A***, ***B***) demonstrate well-defined areas of abnormal high signal in the basal ganglia bilaterally and in a wedge-shaped distribution in the right parietal lobe (*arrows*). Axial (***C***, ***D***) T1-weighted images post-gadiolinium. *(continued)*

Copyright © 2008 The McGraw-Hill Companies. All rights reserved.

E

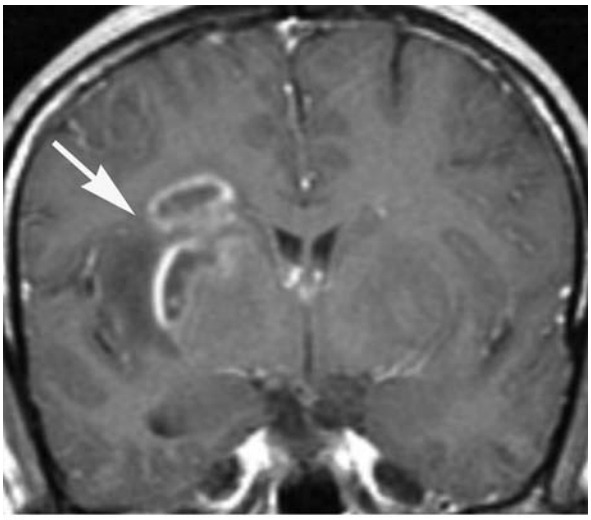

F

FIGURE e30-3 (*Continued*)
Coronal (***E***, ***F***) T1-weighted images post-gadolinium demonstrate irregular ring enhancement of the lesions (*arrows*).

Copyright © 2008 The McGraw-Hill Companies. All rights reserved.

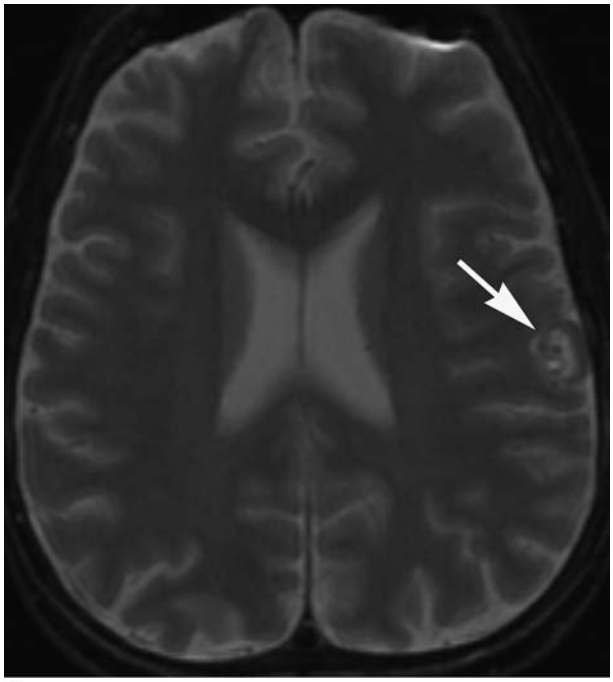

A

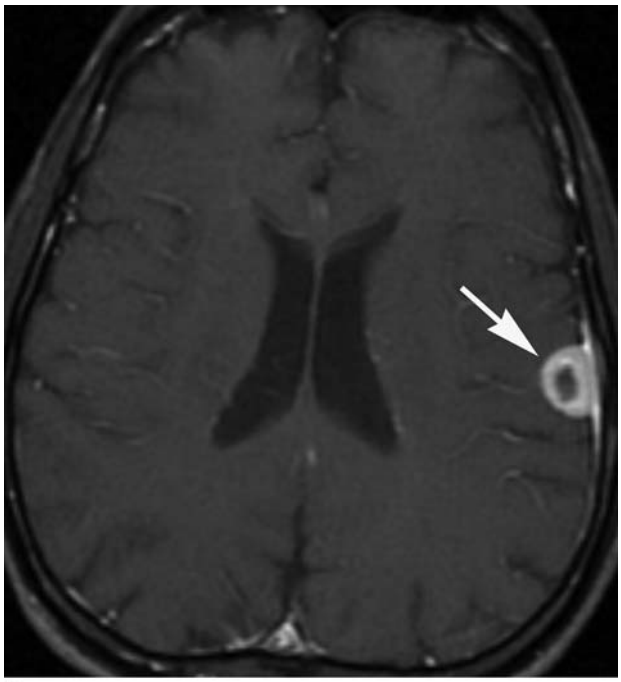

B

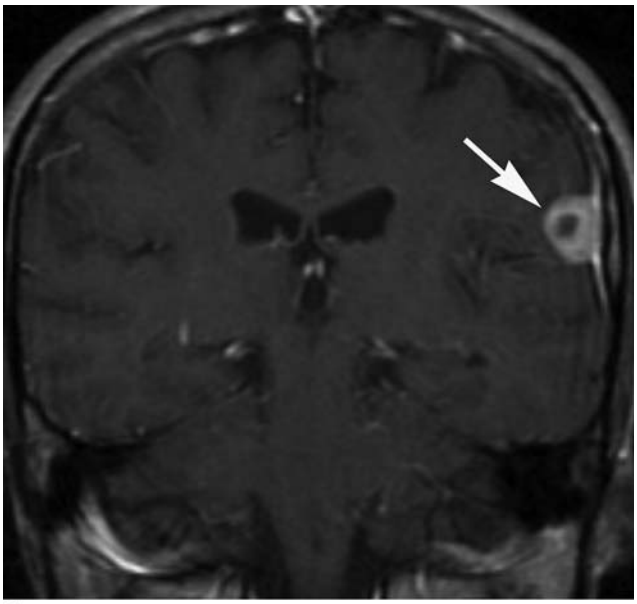

C

FIGURE e30-4 Neurosyphilis (Chap. 162)
Case II
Axial T2-weighted MRI (***A***) demonstrates a dural-based, peripherally hyperintense and centrally hypointense lesion located lateral to the left frontal lobe (*arrows*).
Axial (***B***) and coronal (***C***) T1-weighted MR images post-gadolinium demonstrate peripheral enhancement of the lesion (*arrows*).

Copyright © 2008 The McGraw-Hill Companies. All rights reserved.

A

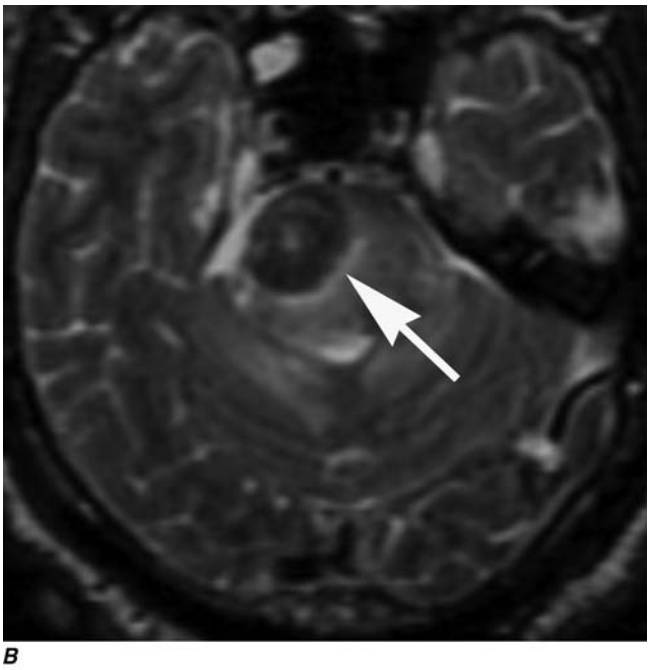

B

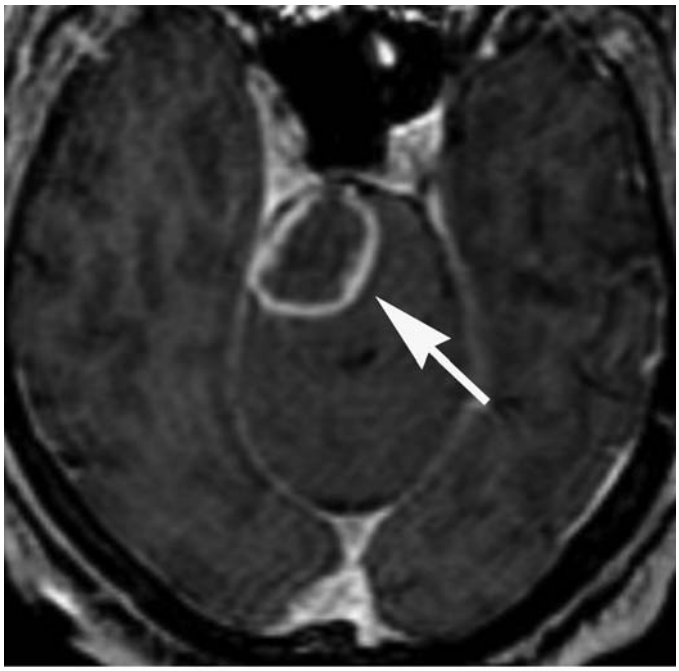

C

FIGURE e30-5 Histoplasmosis of the pons (Chap. 192)
Axial FLAIR (***A***) and T2-weighted (***B***) MR images demonstrate a low signal mass in the right pons (*arrow*) with surrounding vasogenic edema. Axial T1-weighted MR image post-gadolinium (***C***) demonstrates ring enhancement of the lesion in the right pons (*arrows*). Of note, there was no evidence of restricted diffusion (not shown).

Copyright © 2008 The McGraw-Hill Companies. All rights reserved.

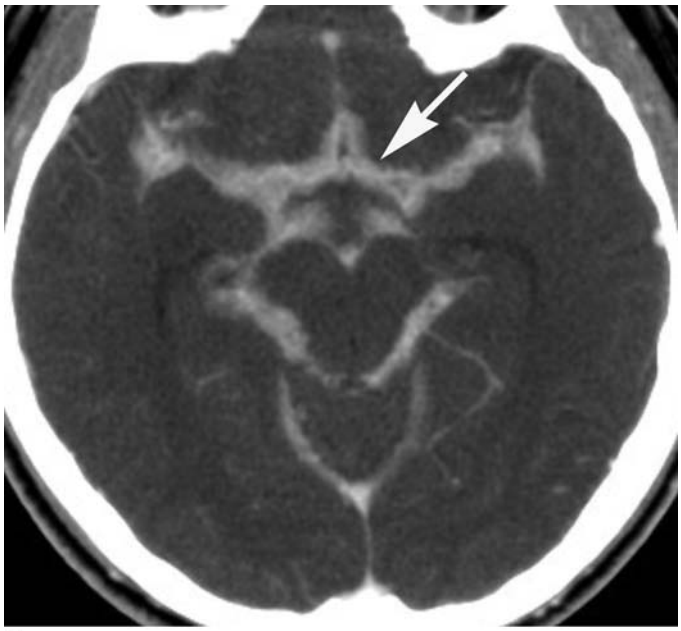

A

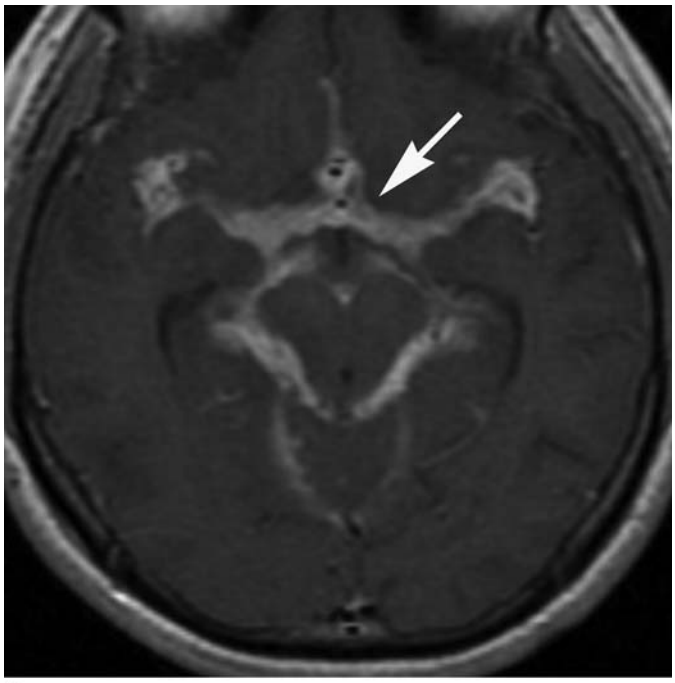

B

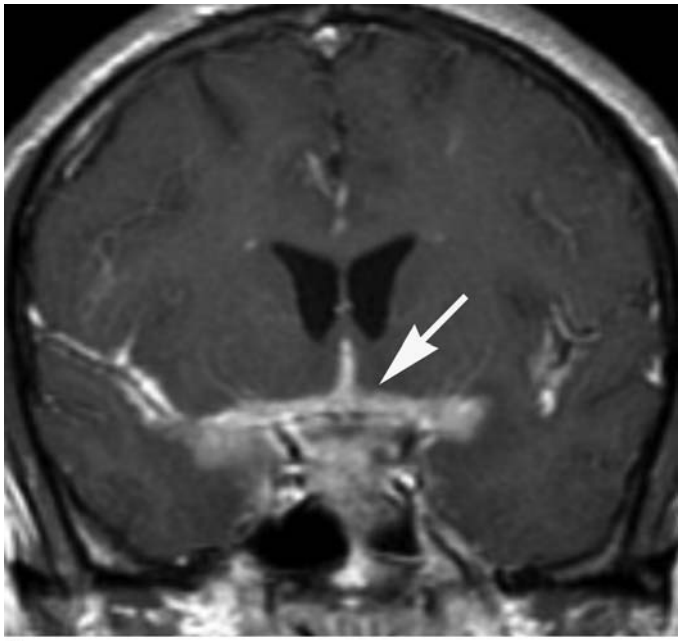

C

FIGURE e30-6 Coccidiomycosis meningitis (Chap. 193)
Axial post-contrast CT (***A***) and axial (***B***) and coronal (***C***) T1-weighted MR images post-gadolinium demonstrate enhancement of the perimesencephalic cisterns (*arrows*), as well as the sylvian and interhemispheric fissures.

Copyright © 2008 The McGraw-Hill Companies. All rights reserved.

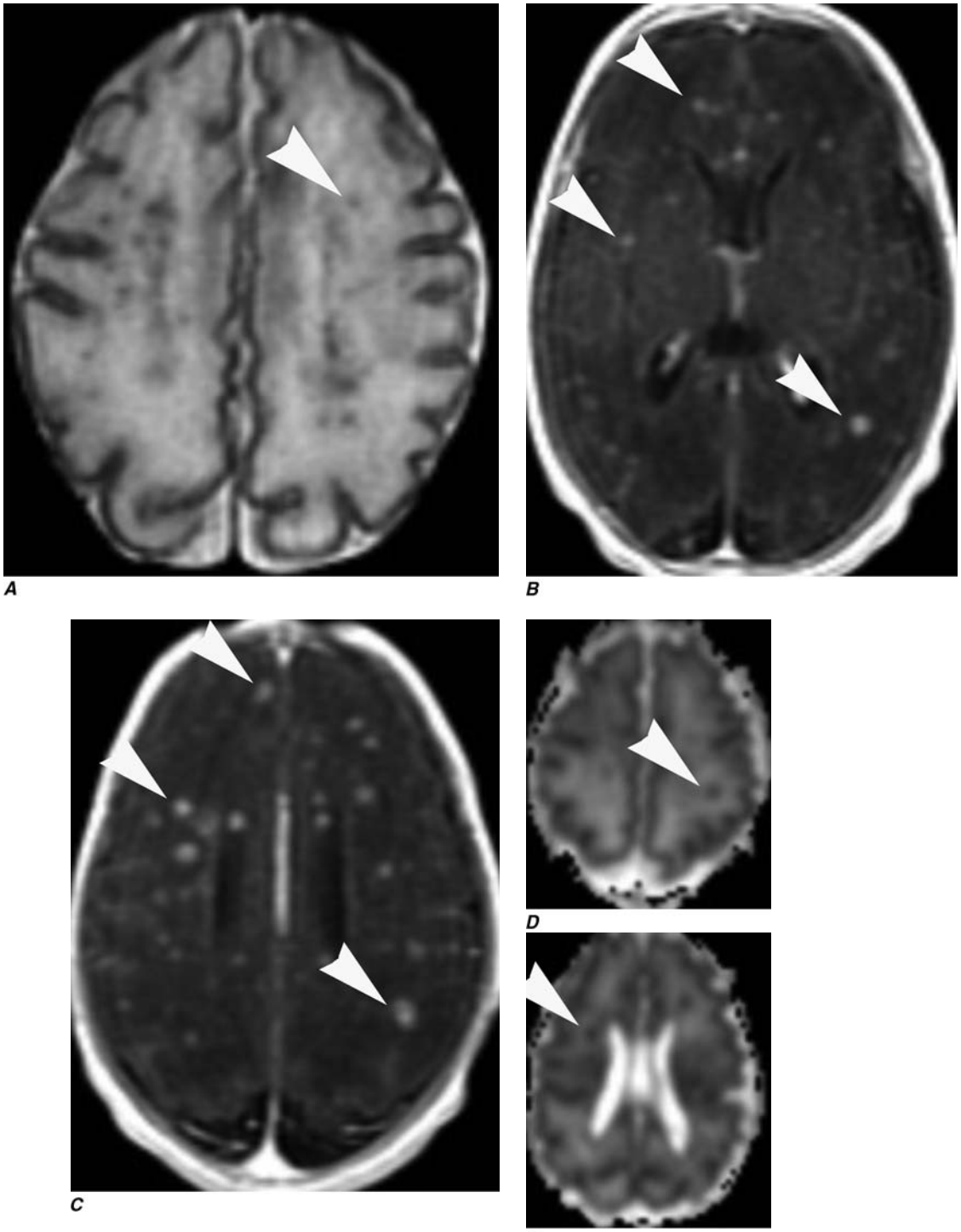

FIGURE e30-7 Candidiasis in a newborn (Chap. 196)
Axial T2-weighted MR image (***A***) demonstrates multiple punctate foci of low signal diffusely distributed in the brain parenchyma (*arrowheads*). Axial T1-weighted MR images post-gadolinium (***B***, ***C***) demonstrate marked enhancement of the lesions (*arrowheads*). ADC map (***D***, ***E***) demonstrates restricted diffusion of water molecules in the lesions (*arrowheads*).

Copyright © 2008 The McGraw-Hill Companies. All rights reserved.

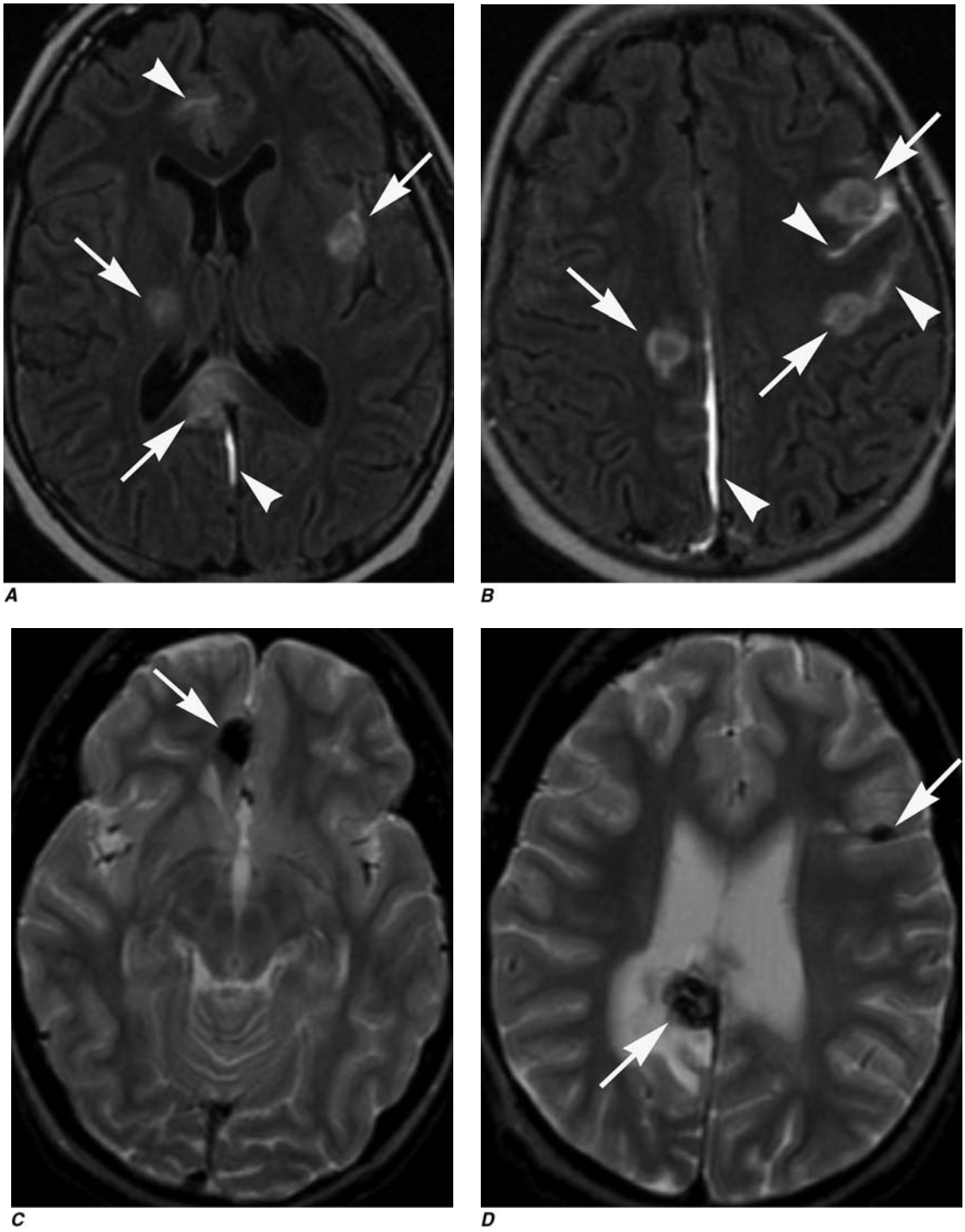

FIGURE e30-8 CNS aspergillosis (Chap. 197)
Axial FLAIR MR images (***A***, ***B***) demonstrate multiple areas of abnormal high signal in the basal ganglia as well as cortex and subcortical white matter (*arrows*). There is also abnormal high signal in the subarachnoid space adjacent to the lesions (*arrowhead*) that can correspond to blood or high protein content. Axial T2-weighted MR images (***C***, ***D***) demonstrate intrinsic low signal in the lesions (*arrows*), suggesting the presence of blood products. Some of the lesions also show vasogenic edema. *(continued)*

Copyright © 2008 The McGraw-Hill Companies. All rights reserved.

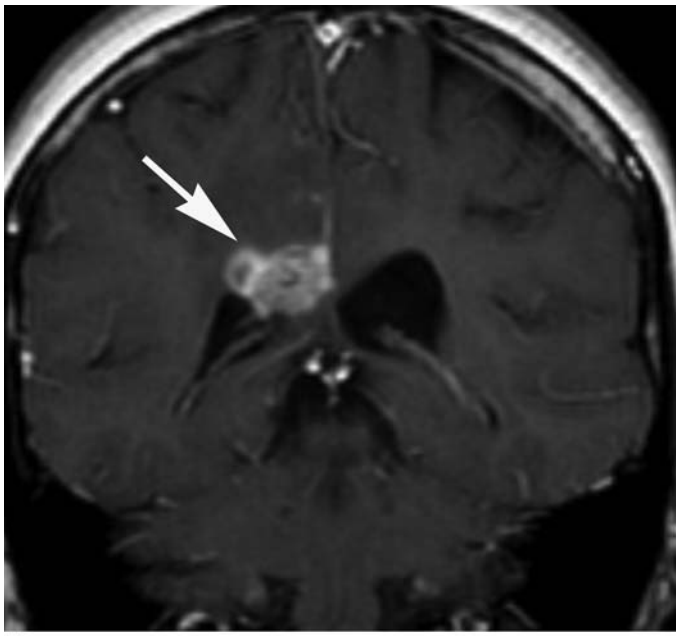

E

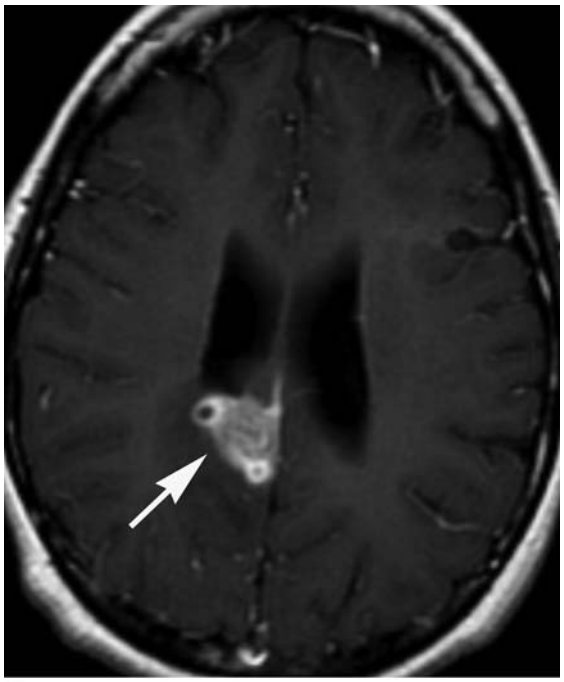

F

FIGURE e30-8 (*Continued*)
Coronal (***E***) and axial (***F***) T1-weighted MR images post-gadolinium demonstrate peripheral enhancement of the lesions (*arrows*).

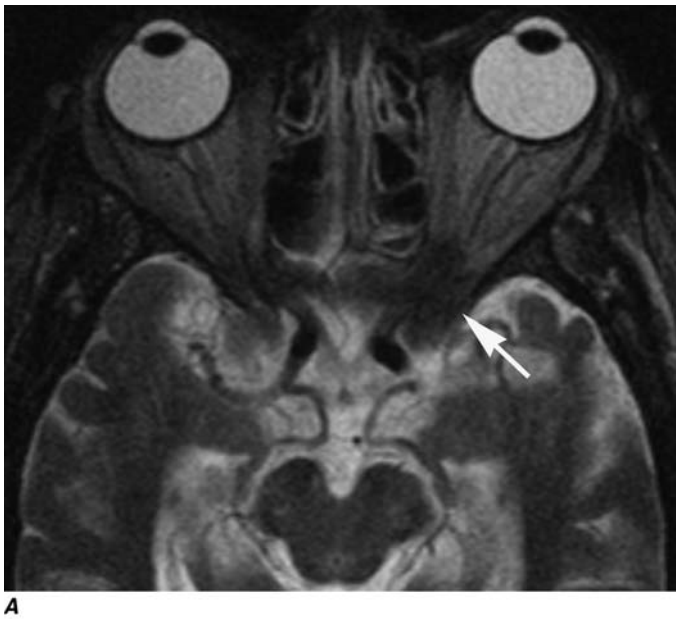

A

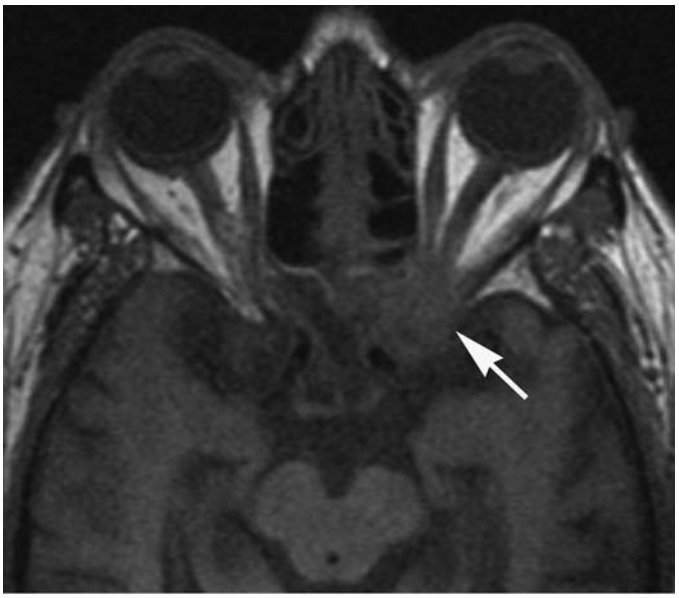

B

FIGURE e30-9 Invasive sinonasal aspergillosis (Chap. 197)
Axial T2-weighted MR image (***A***) demonstrates an irregularly shaped low signal lesion involving the left orbital apex (*arrow*).

B. T1-weighted image pre-gadolinium demonstrates enhancement of lesion (*arrow*). *(continued)*

Copyright © 2008 The McGraw-Hill Companies. All rights reserved.

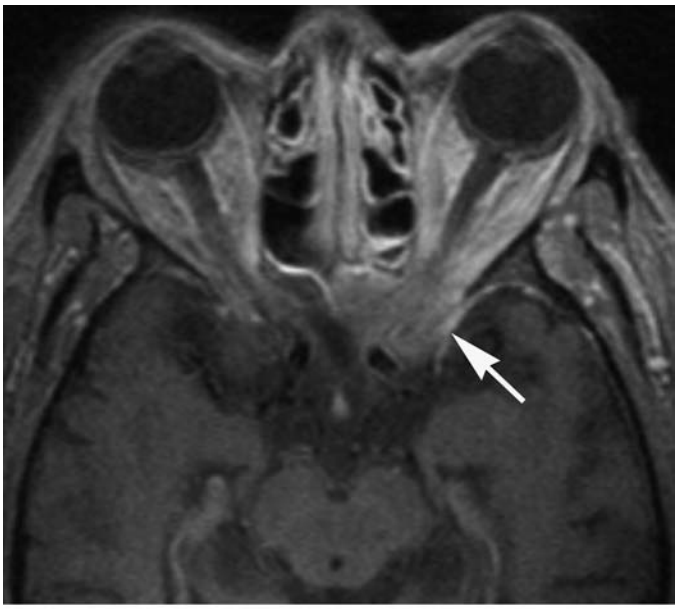

C

FIGURE e30-9 (*Continued*)
C. T1-weighted image post-gadolinium demonstrates enhancement of lesion (*arrow*).

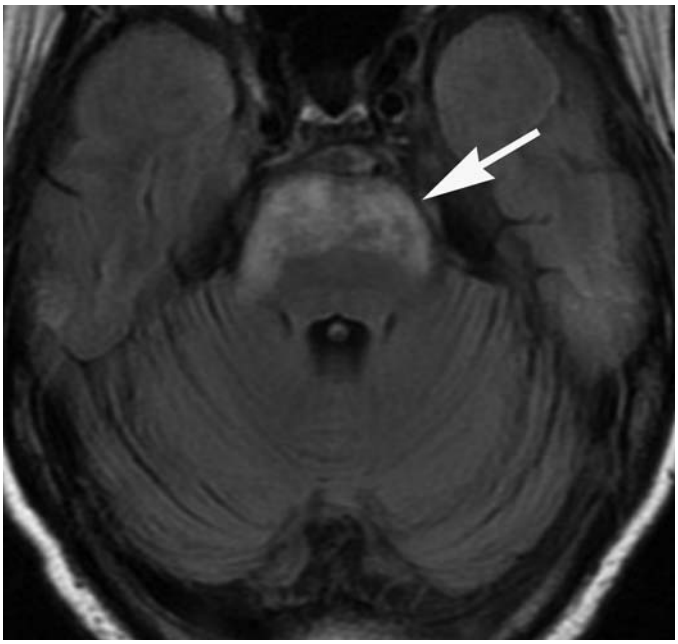

FIGURE e30-10 Behçet's disease (Chap. 320)
Axial FLAIR MRI demonstrates abnormal high signal involving the anterior pons (*arrow*); following gadolinium administration, the lesion was nonenhancing (not shown). Brainstem lesions are typical of Behçet's disease, caused primarily by vasculitis and in some cases demyelinating lesions.

Copyright © 2008 The McGraw-Hill Companies. All rights reserved.

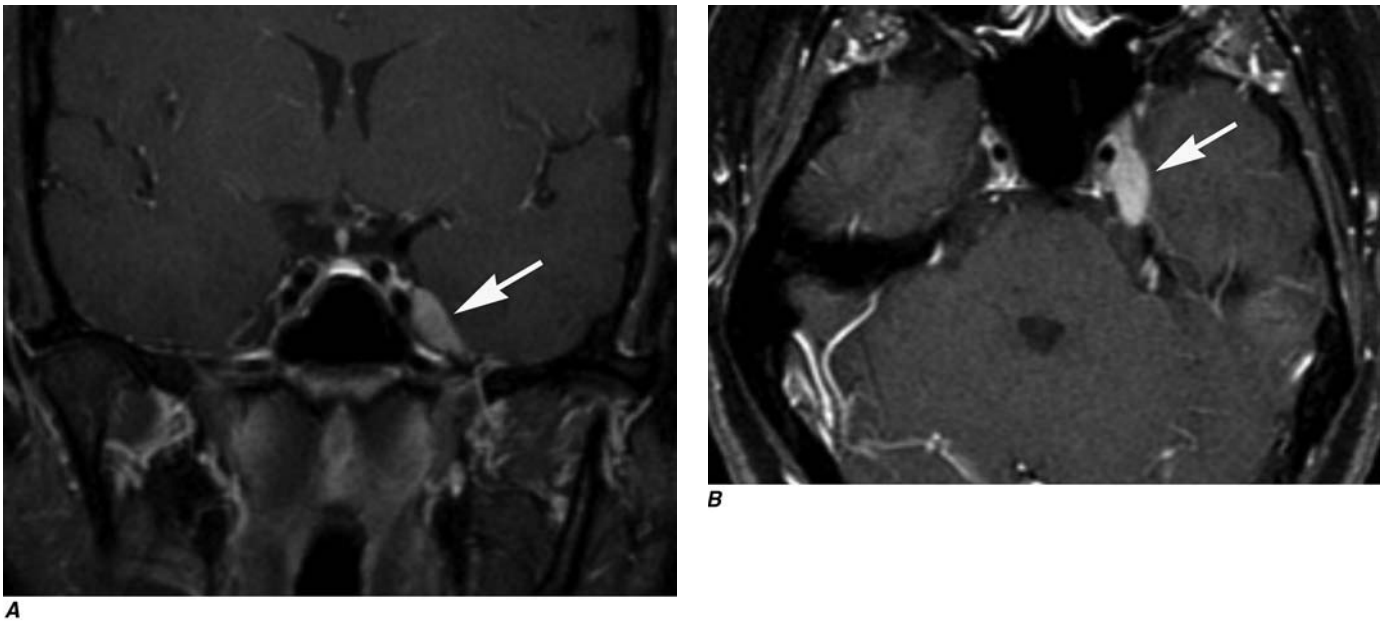

FIGURE e30-11 Neurosarcoid (Chap. 322)
Case I
Axial (***A***) and coronal (***B***) T1-weighted images post-gadolinium with fat suppression demonstrate a homogeneously enhancing well circumscribed mass centered in the left Meckel's cave (*arrows*).

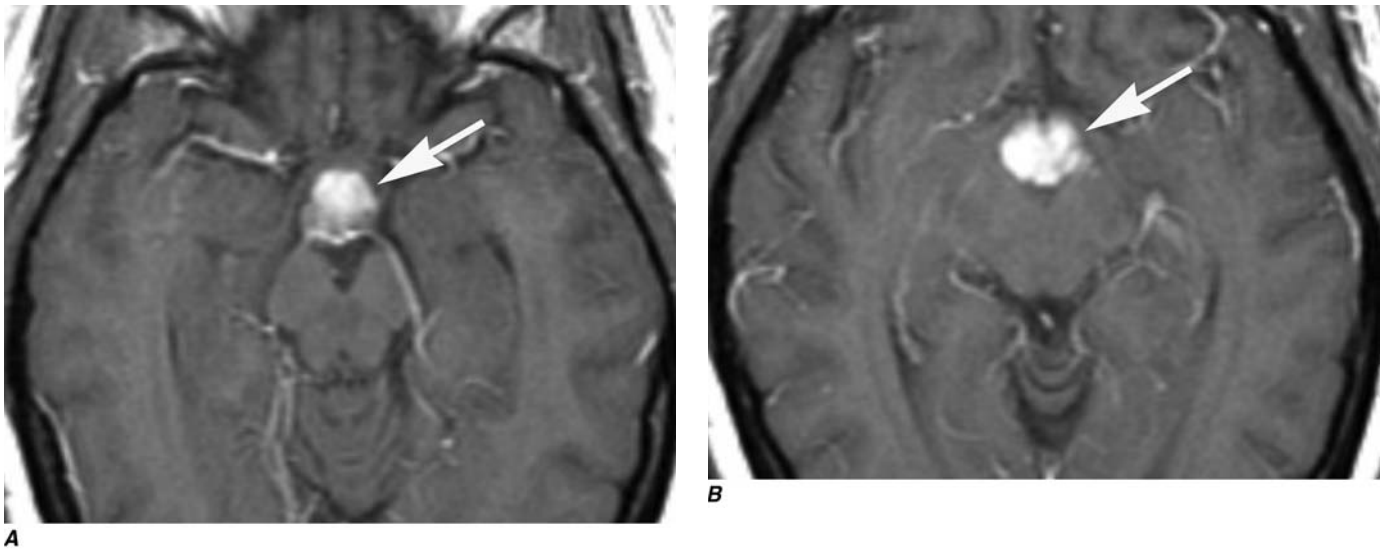

FIGURE e30-12 Neurosarcoid (Chap. 322)
Case II
Axial (***A***, ***B***) and sagittal (***C***) T1-weighted images post-gadolinium with fat suppression demonstrate a homogeneously enhancing mass involving the hypothalamus and the pituitary stalk (*arrows*). *(continued)*

Copyright © 2008 The McGraw-Hill Companies. All rights reserved.

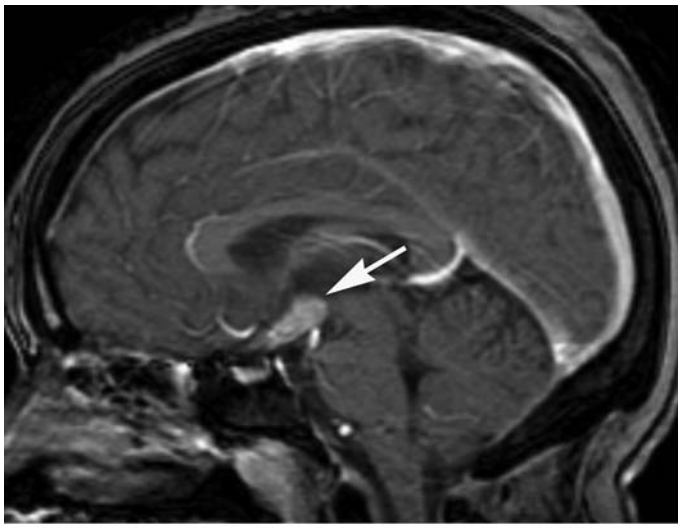

C

FIGURE e30-12 (*Continued*)

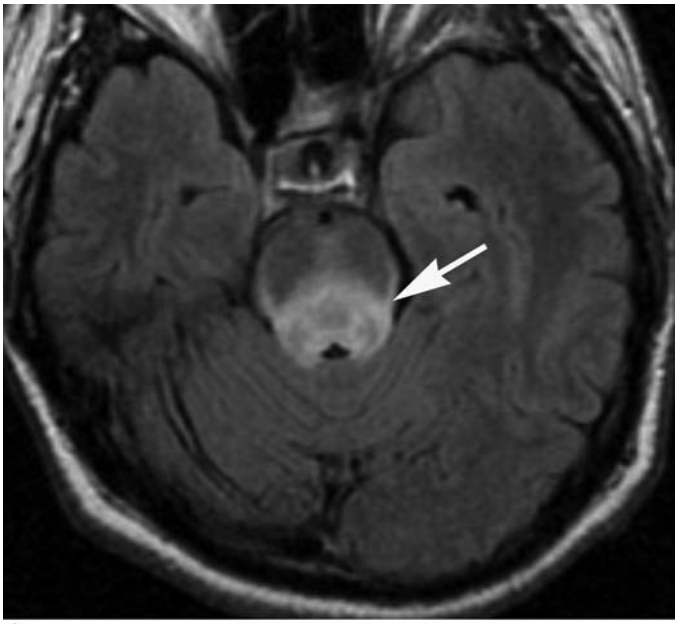

A

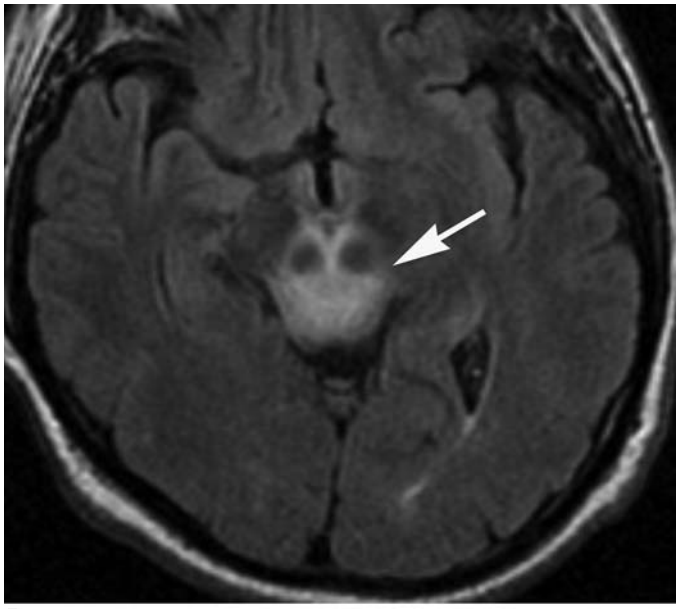

B

FIGURE e30-13 Neurosarcoid (Chap. 322)
Case III
Axial FLAIR images (***A–E***) demonstrate abnormal high signal and slight expansion in the midbrain, dorsal pons, and pineal region (*arrows*) without significant mass effect. *(continued)*

Copyright © 2008 The McGraw-Hill Companies. All rights reserved.

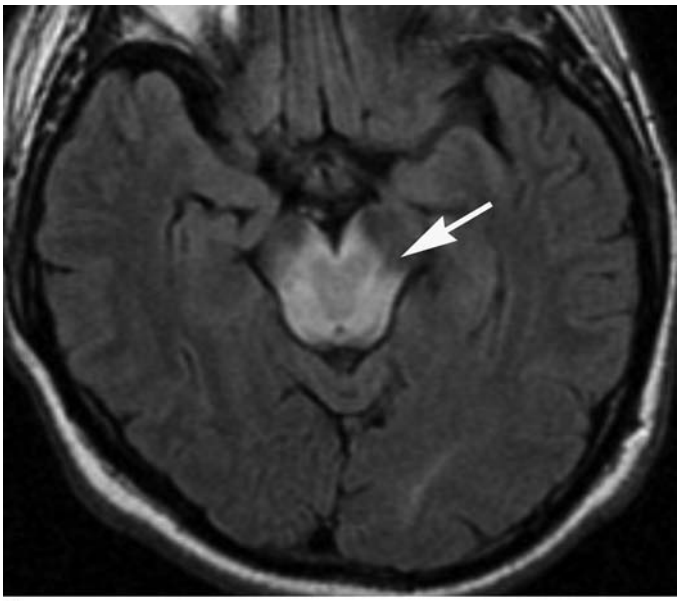

C

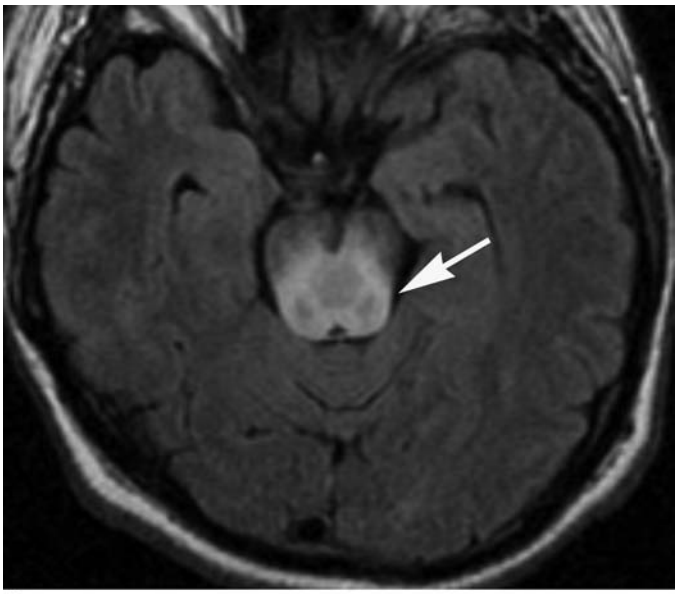

D

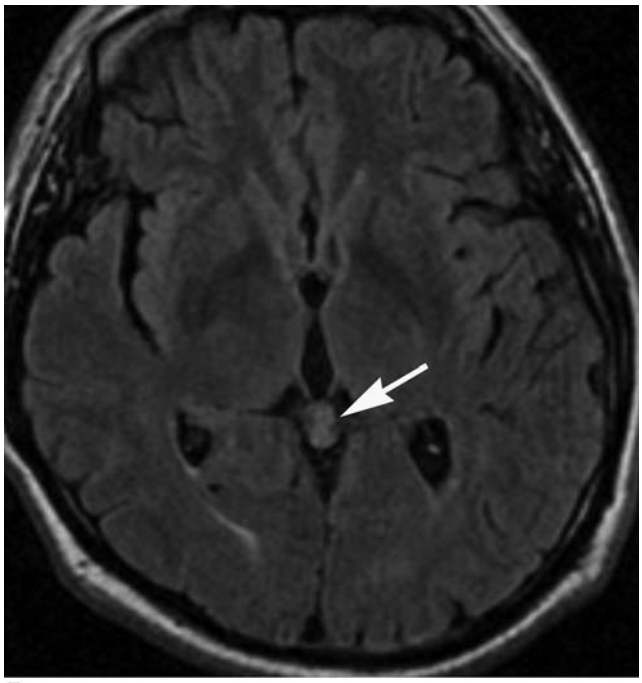

E

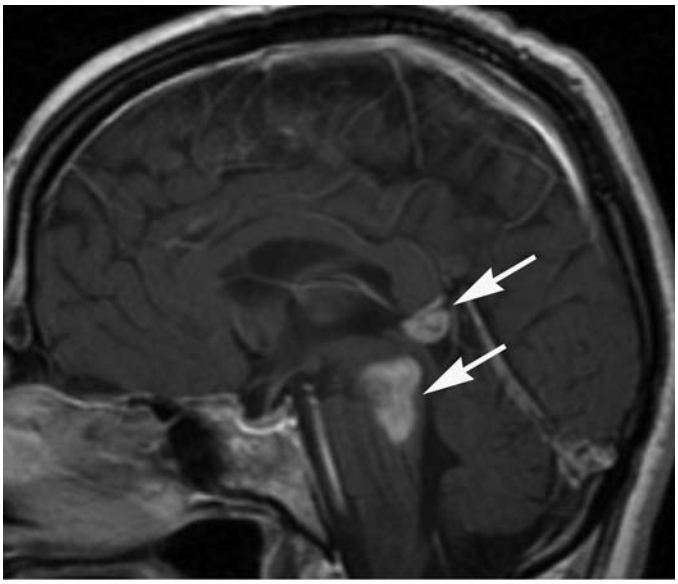

F

FIGURE e30-13 (*Continued*)
Sagittal T1-weighted images post-gadolinium (***F***) with fat suppression demonstrate abnormal enhancement in the midbrain, dorsal pons, and pineal region (*arrows*).

Copyright © 2008 The McGraw-Hill Companies. All rights reserved.

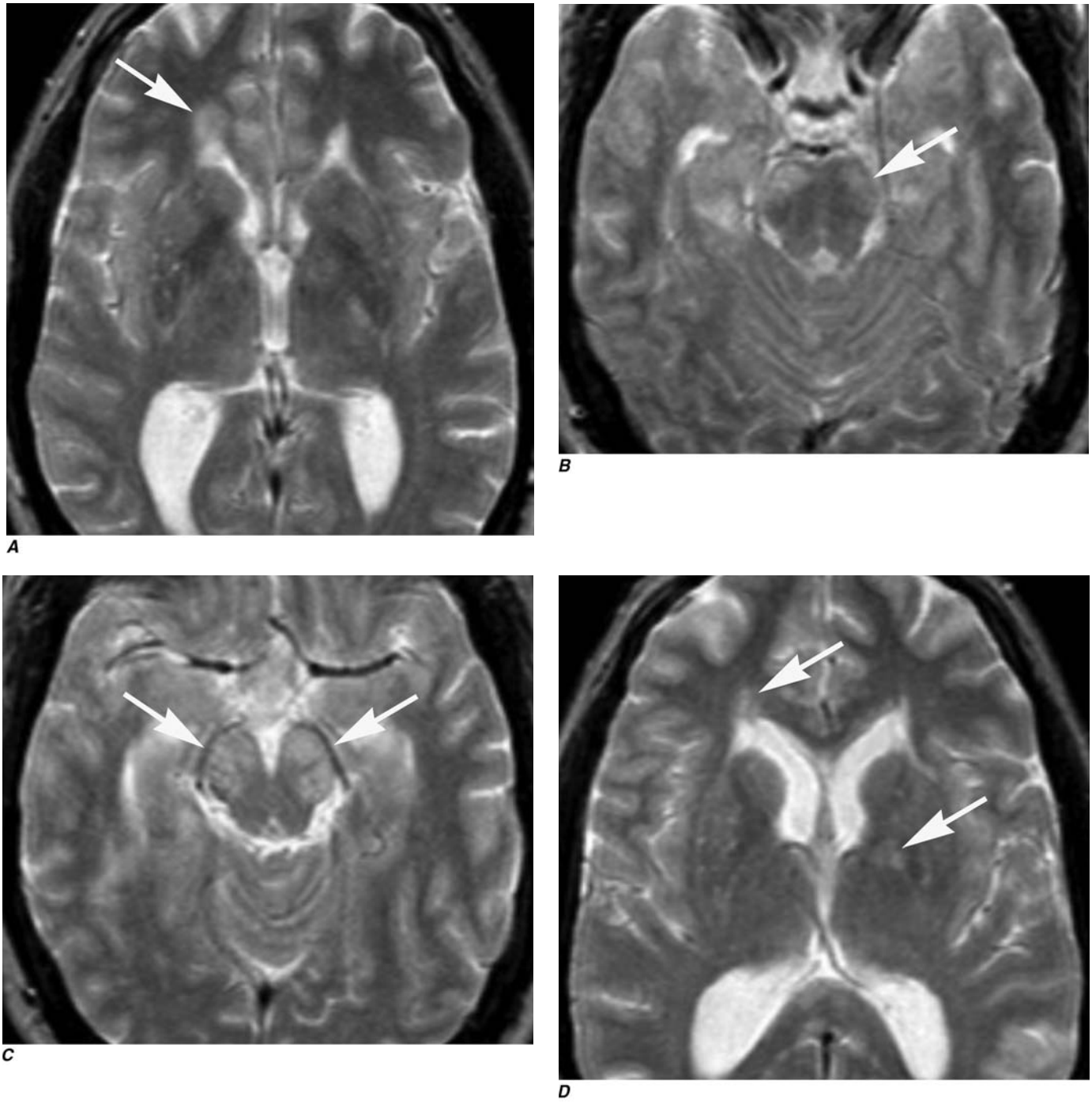

FIGURE e30-14 Neurosarcoid (Chap. 322)
Case IV
Axial T2-weighted images (***A–D***) demonstrate numerous areas of abnormal hyperintensity involving the corpus callosum, left internal capsule and globus pallidus, bilateral cerebral peduncles, bilateral gyrus rectus, right frontal lobe periventricular white matter, and patchy areas in bilateral temporal lobes. *(continued)*

Copyright © 2008 The McGraw-Hill Companies. All rights reserved.

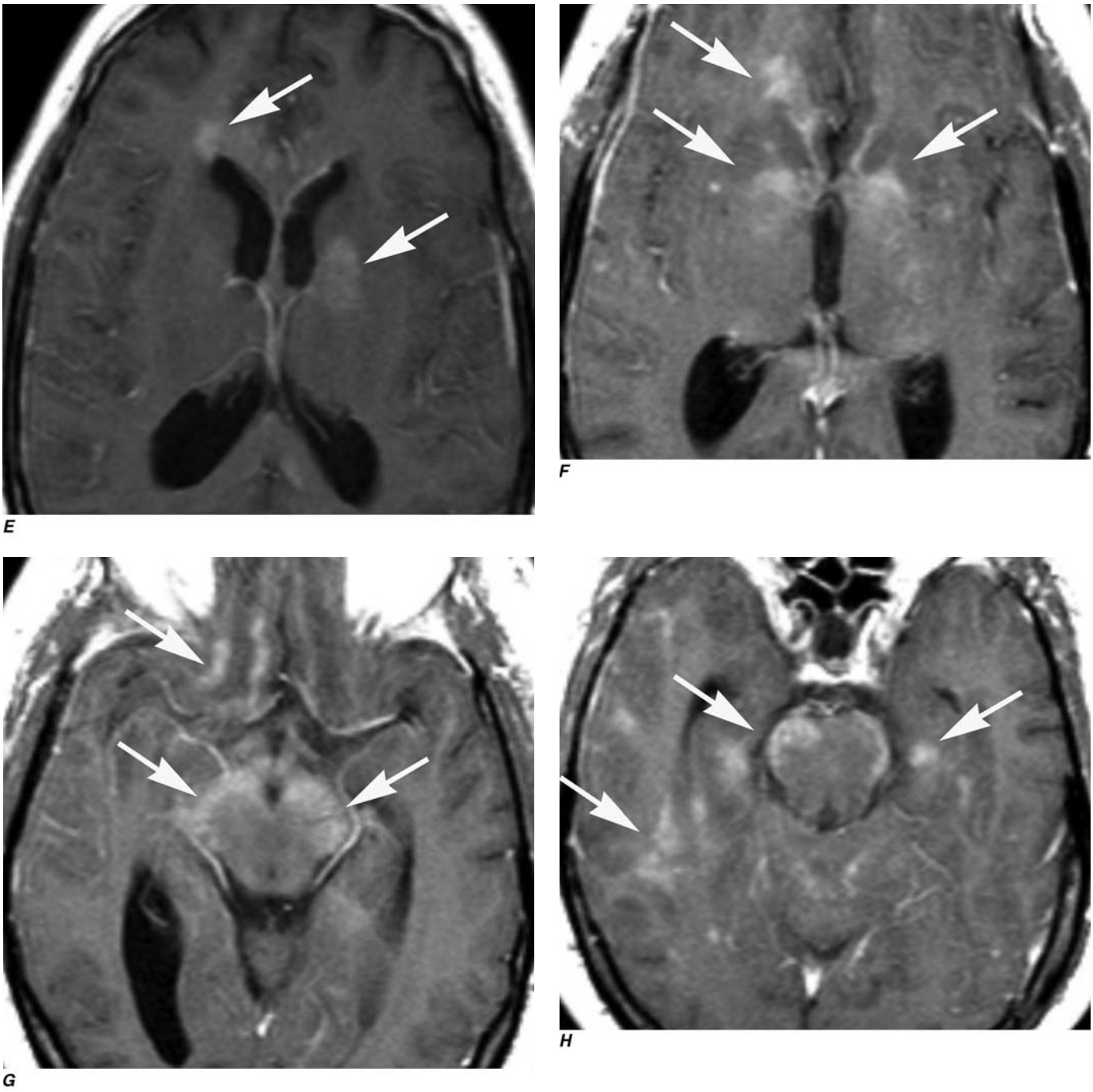

FIGURE e30-14 (*Continued*)
T1-weighted images post-gadolinium (***E–H***) demonstrate abnormal enhancement of those areas with high T2 signal.

Copyright © 2008 The McGraw-Hill Companies. All rights reserved.

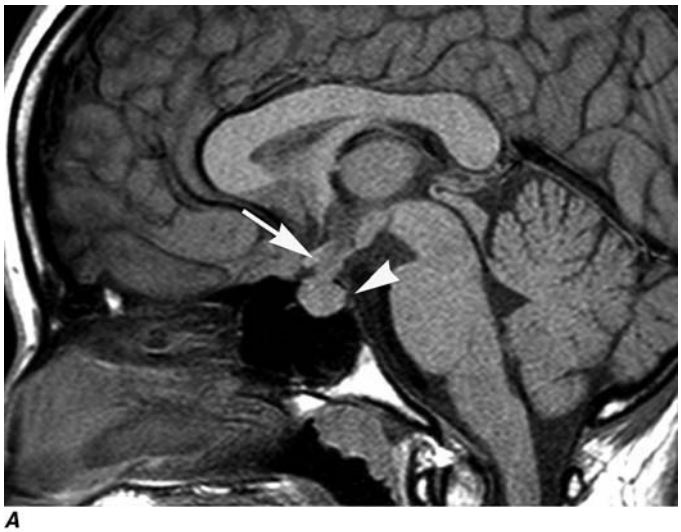

A

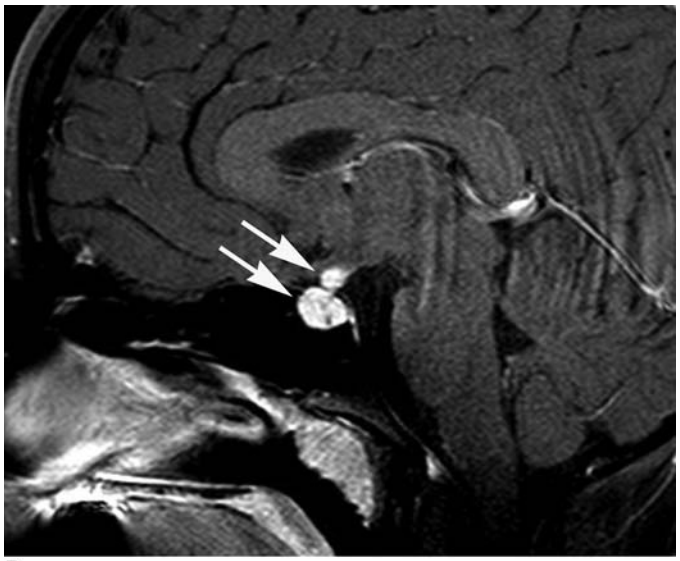

B

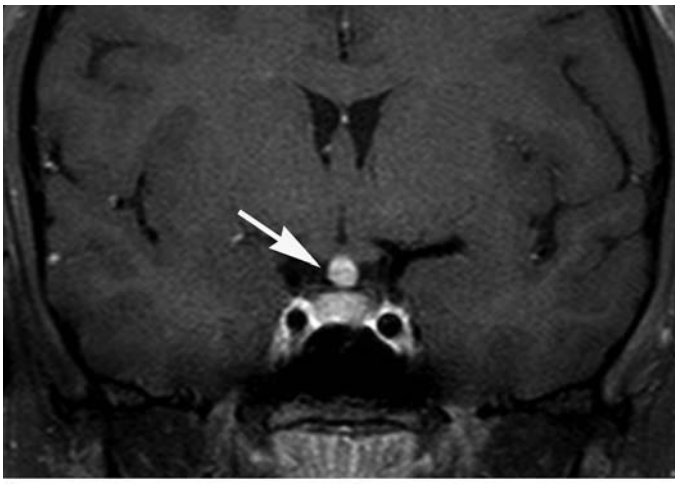

C

FIGURE e30-15 Histiocytosis (Chap. 334)
Sagittal T1-weighted image (***A***) demonstrates enlargement of the pituitary stalk (*arrow*) and absence of the posterior pituitary intrinsic T1 hyperintensity (*arrowhead*).
Sagittal and coronal T1-weighted images post-gadolinium (***B***, ***C***) demonstrate enhancement of the pituitary stalk and infundibulum (*arrows*).

Copyright © 2008 The McGraw-Hill Companies. All rights reserved.

A

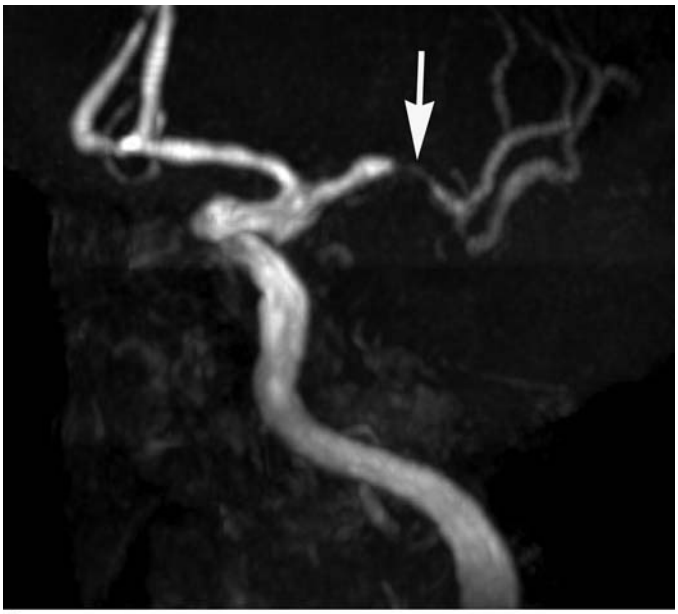

B

FIGURE e30-16 Middle cerebral artery stenosis (Chap. 364) Time-of-flight (TOF) MR angiography (MRA) (***A***, ***B***) reveals narrowing within the left M1 segment that is likely secondary to atherosclerosis (*arrows*).

Copyright © 2008 The McGraw-Hill Companies. All rights reserved.

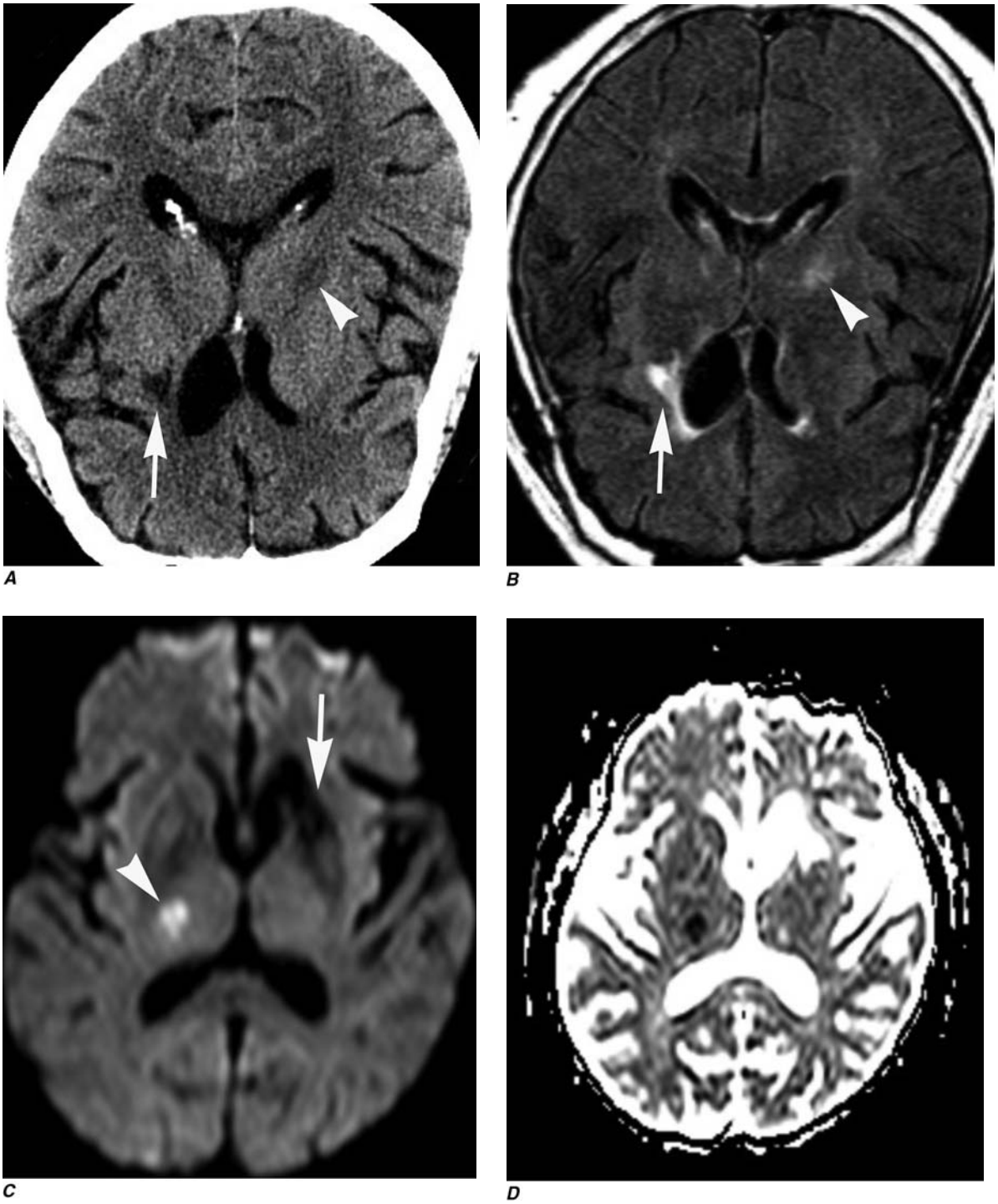

FIGURE e30-17 Lacunar infarction (Chap. 364)
Axial noncontrast CT (***A***) demonstrates abnormal hypodensity involving the left anterior putamen and anterior limb of internal capsule with ex-vacuo dilatation of the adjacent frontal horn of the left lateral ventricle, suggestive of an old infarction (*arrow*). A small area of slight hypodensity is also seen in the posterior limb of the right internal capsule that can correspond to an acute infarct (*arrowhead*).
Axial FLAIR MRI (***B***) demonstrates abnormal high signal involving the left anterior putamen and anterior limb of internal capsule with ex-vacuo dilatation of the adjacent frontal horn of the left lateral ventricle, suggestive of an old infarction (*arrow*). A small area of slight hyperintensity is also seen in the posterior limb of the right internal capsule that can correspond to an acute lacunar infarct (*arrowhead*).
Diffusion-weighted image (***C***) and apparent diffusion coefficient (ADC) map (***D***) demonstrate restricted water motion in the lesion of the posterior limb of the right internal capsule, strongly suggestive for an acute lacunar infarct (*arrowhead*). There is no evidence of restricted diffusion in the old infarct (*arrow*).

Copyright © 2008 The McGraw-Hill Companies. All rights reserved.

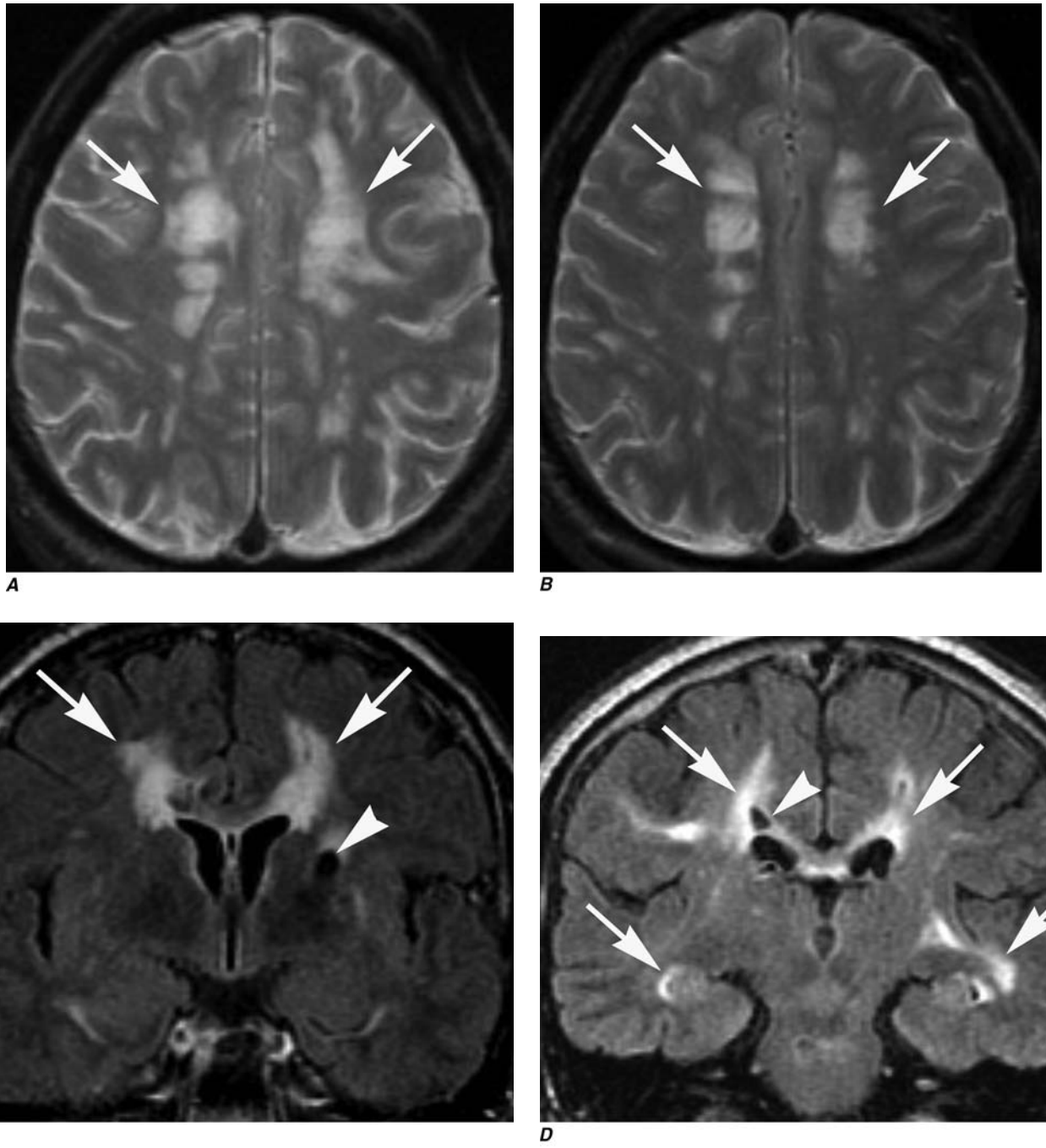

FIGURE e30-18 Cerebral autosomal dominant arteriopathy with subcortical infarcts and leukoencephalopathy (CADASIL) (Chap. 364)

Axial T2-weighted MR images (***A***, ***B***) demonstrate multiple patchy areas of abnormal high signal in the periventricular white matter (*arrows*). Coronal FLAIR MRI (***C***, ***D***) demonstrates multiple patchy areas of abnormal high signal in the periventricular white matter bilaterally, including the temporal lobes (*arrows*). In some of these areas, there are small areas of tissue loss (encephalomalacia) (*arrowheads*).

Copyright © 2008 The McGraw-Hill Companies. All rights reserved.

A

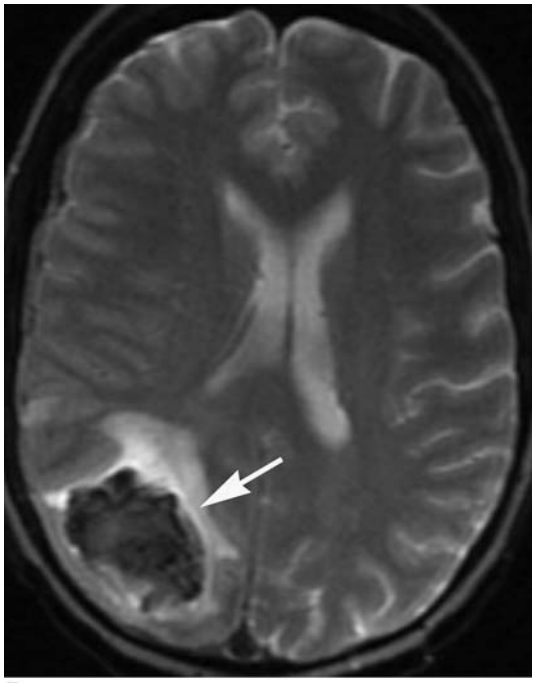

B

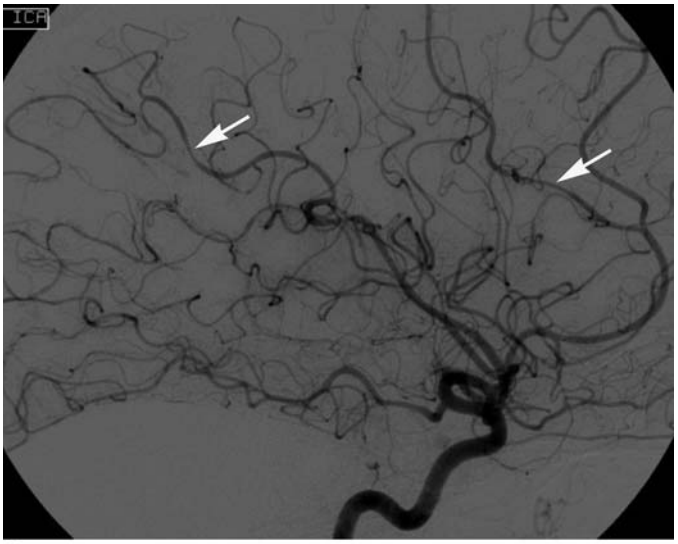

C

FIGURE e30-19 CNS vasculitis (Chap. 364)
Axial noncontrast CT (***A***) demonstrates a large hyperdense intraparenchymal hematoma surrounded by hypodense vasogenic edema in the right parietal lobe.
Axial T2-weighted MRI (***B***) demonstrates a large hypointense intraparenchymal hematoma surrounded by hyperintense vasogenic edema in the right parietal lobe.
Conventional angiography (***C***) demonstrates multiple segments of intracranial arterial narrowing, some of which have associated adjacent areas of focal arterial dilatation. These abnormalities are suggestive of vasculitis.

Copyright © 2008 The McGraw-Hill Companies. All rights reserved.

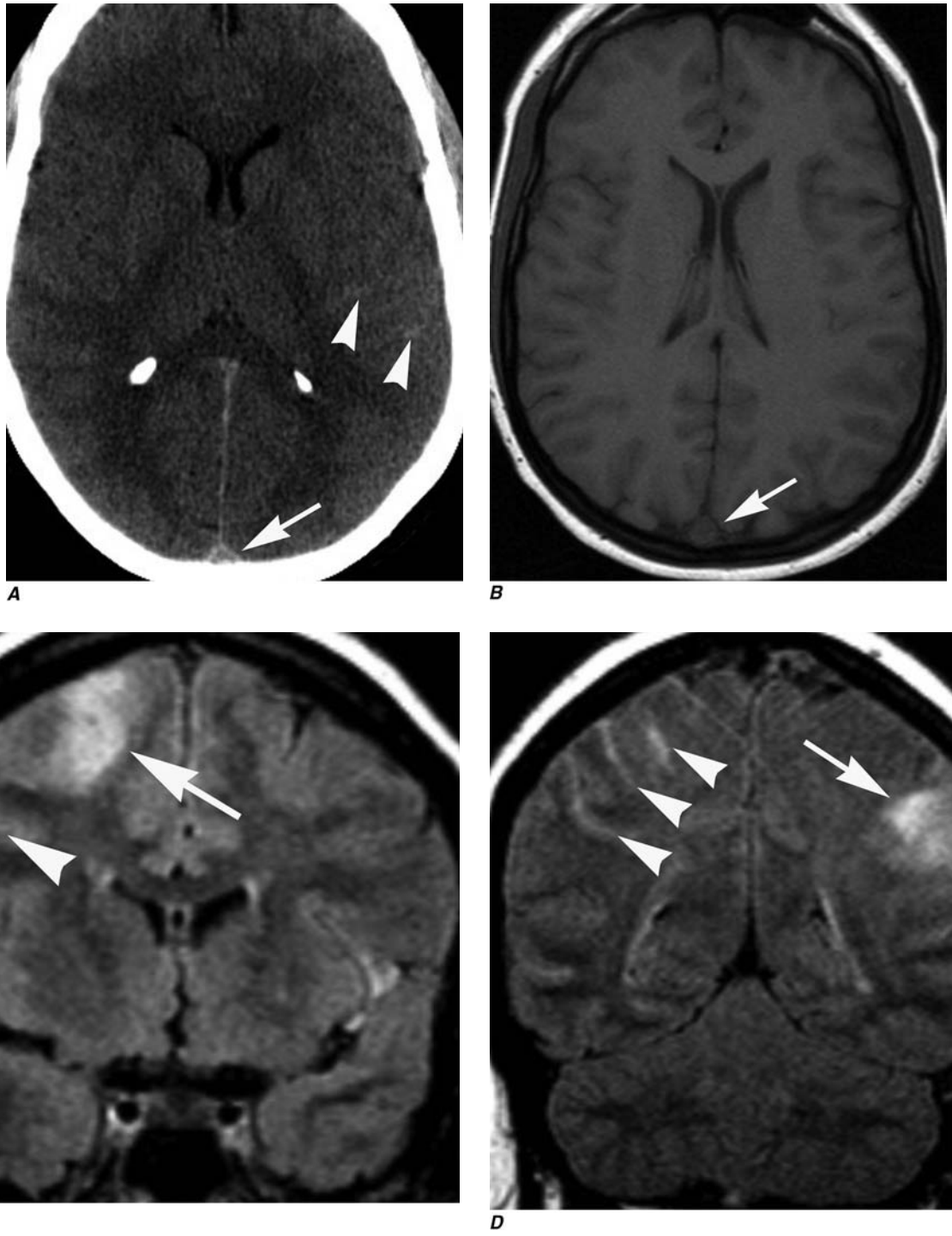

FIGURE e30-20 Superior sagittal sinus thrombosis (Chap. 364) Noncontrast CT of the head (***A***) demonstrates increased density in the superior sagittal sinus, suggestive of thrombosis (*arrow*), and small linear hyperdensities in some temporal lobe sulci, suggestive of subarachnoid hemorrhage (*arrowheads*).
Axial T1-weighted MRI (***B***) demonstrates absence of flow void in the superior sagittal sinus, suggestive of thrombosis.
Coronal FLAIR images (***C***, ***D***) demonstrate areas of abnormal high signal involving the gray and the subcortical white matter of the right frontal and left parietal lobes, as well as the adjacent sulci. These findings are suggestive of vasogenic edema with subarachnoid hemorrhage (*arrowheads*). *(continued)*

Copyright © 2008 The McGraw-Hill Companies. All rights reserved.

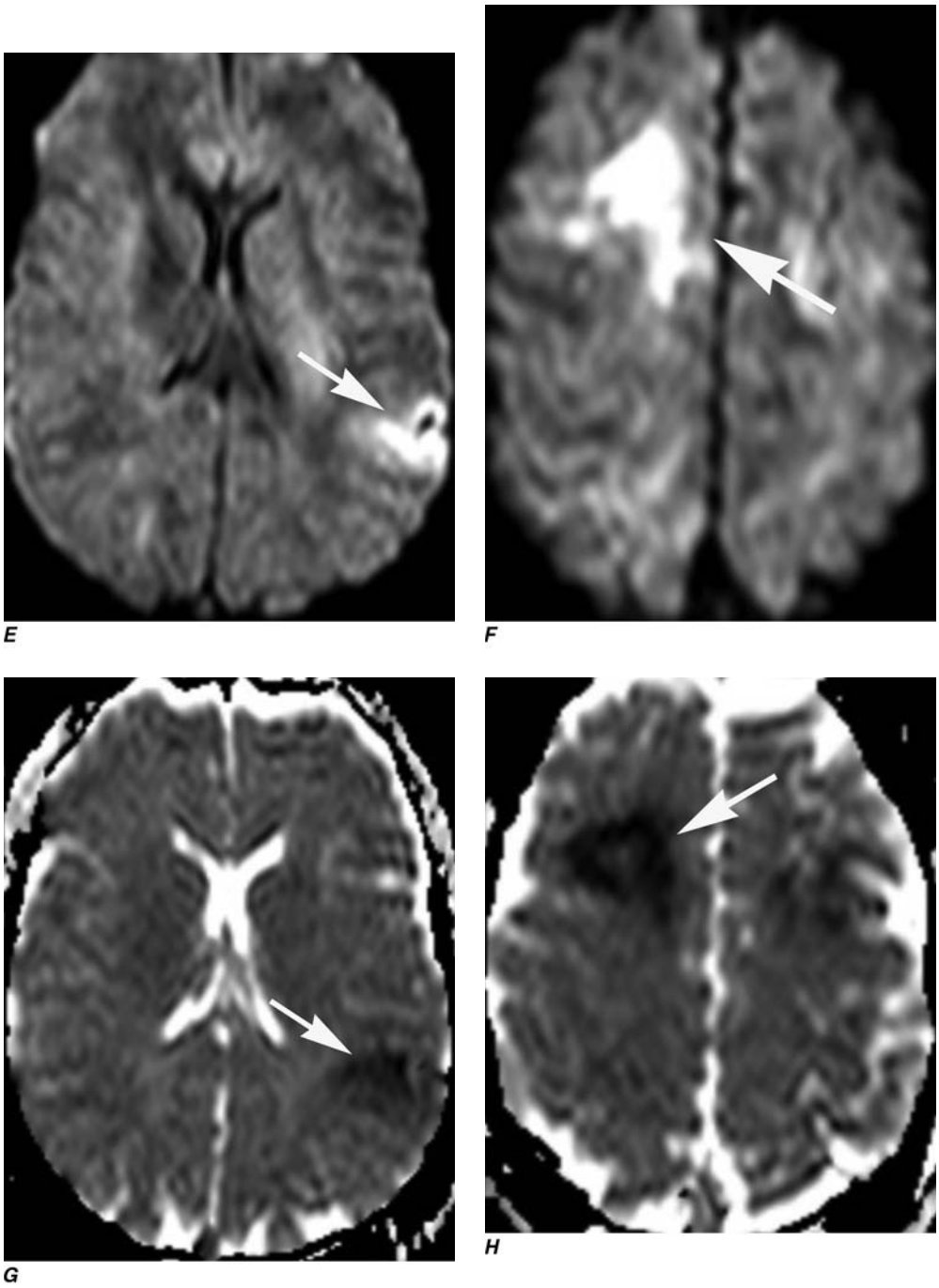

FIGURE e30-20 (*Continued*)
Diffusion-weighted images (***E***, ***F***) and ADC maps (***G***, ***H***) demonstrate restricted diffusion of the abnormal areas on FLAIR, suggestive of infarct. *(continued)*

Copyright © 2008 The McGraw-Hill Companies. All rights reserved.

I

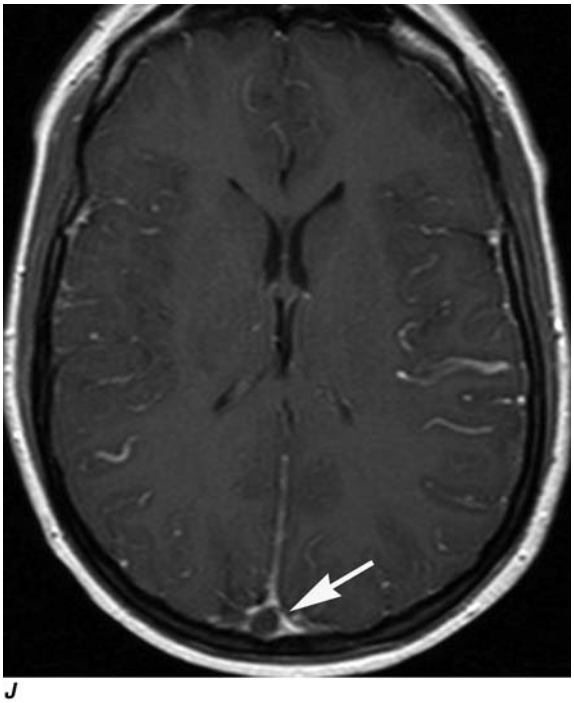

J

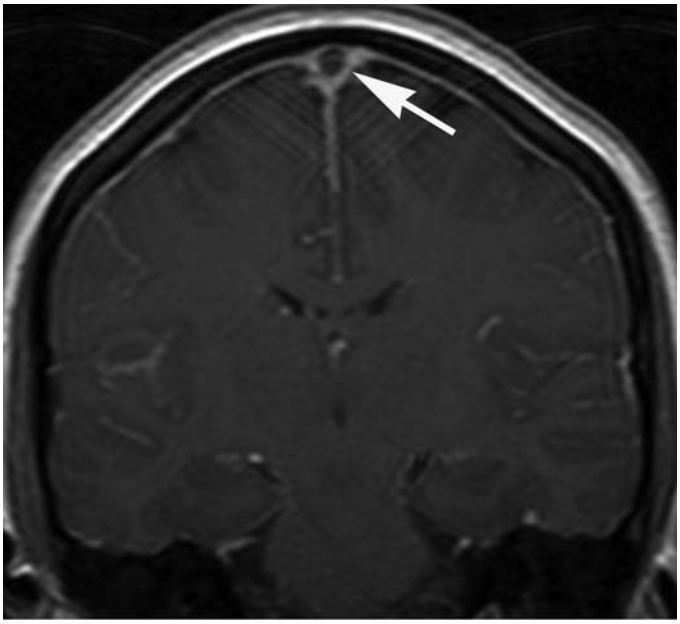

K

FIGURE e30-20 (*Continued*)
Phase-contrast venography of the brain (***I***) demonstrates absence of signal in the superior sagittal sinus down to the torcular herophili, and left transverse sinus and jugular vein.
Axial (***J***) and coronal (***K***) T1-weighted images post-gadolinium demonstrate a filling defect in the superior sagittal sinus, suggestive of thrombosis.

Copyright © 2008 The McGraw-Hill Companies. All rights reserved.

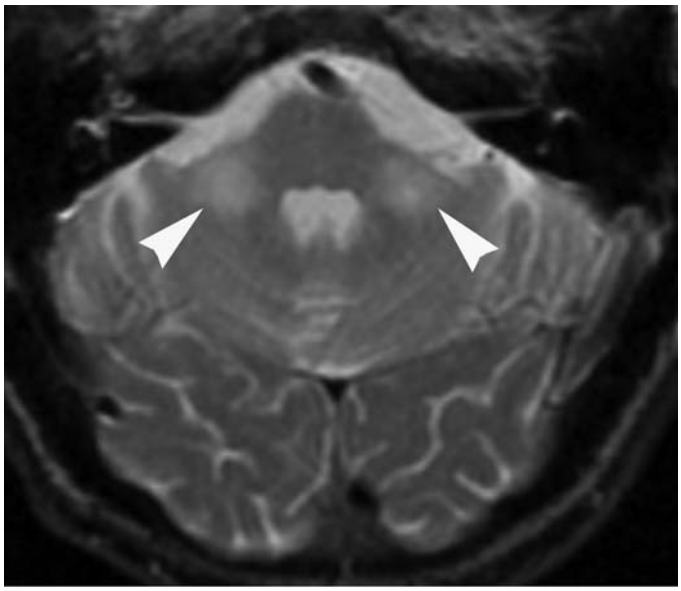

A

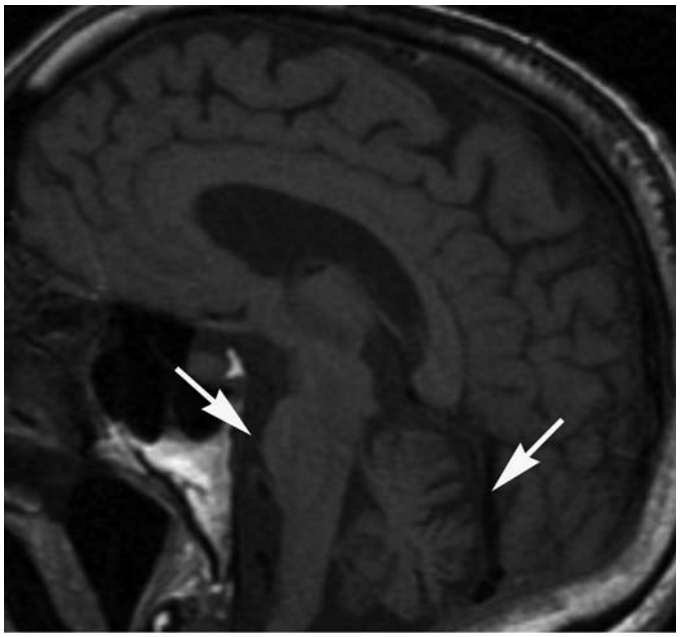

B

FIGURE e30-21 Multiple system atrophy (Chap. 366)
Axial T2-weighted MR image (***A***) reveals symmetric poorly circumscribed abnormal high signal in the middle cerebellar peduncles bilaterally (*arrowheads*). Sagittal T1-weighted MR image (***B***) demonstrates pontine atrophy and enlarged cerebellar fissures as a result of cerebellar atrophy (*arrows*).

Copyright © 2008 The McGraw-Hill Companies. All rights reserved.

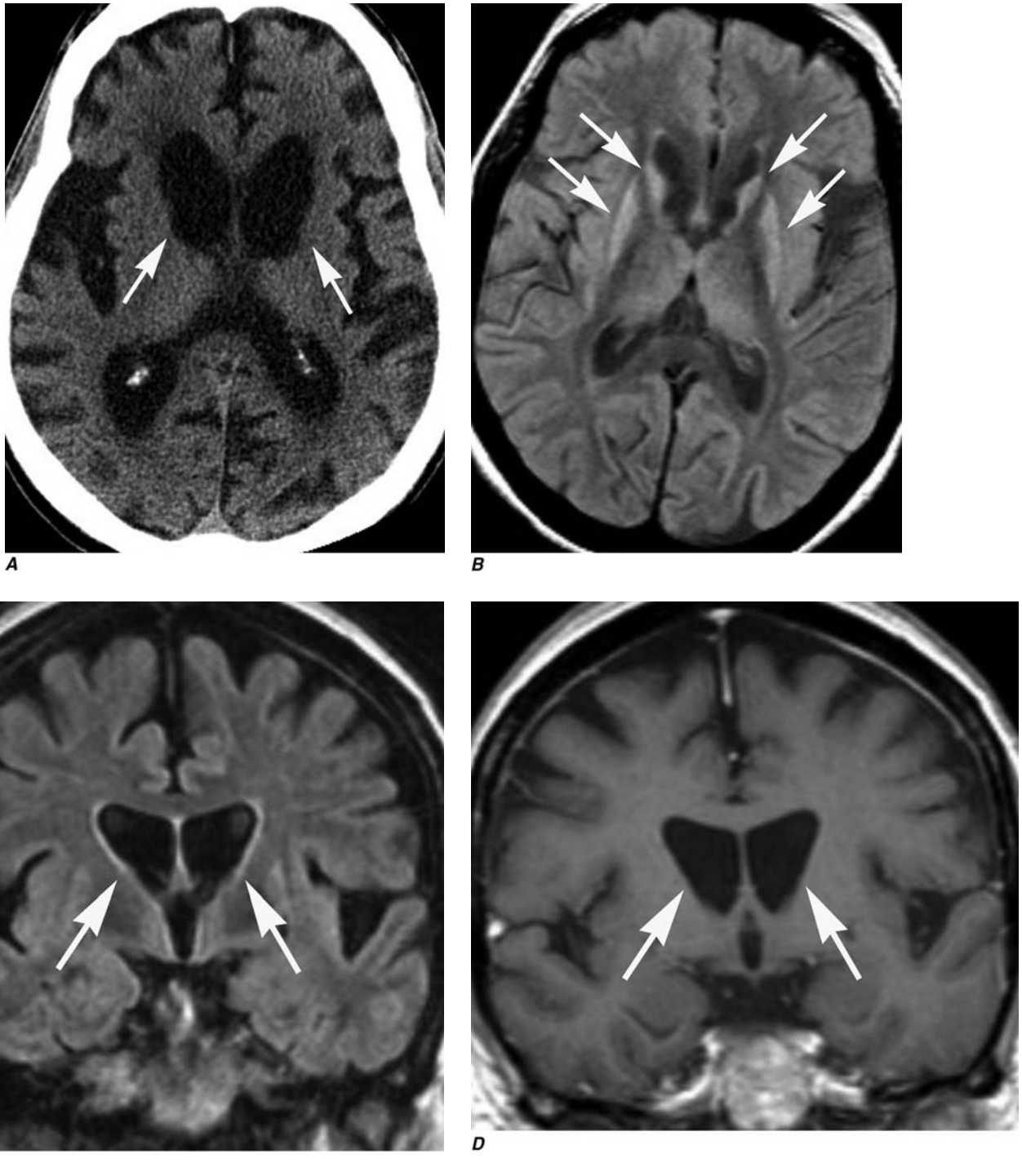

FIGURE e30-22 Huntington's disease (Chap. 367)
Axial noncontrast CT (***A***) demonstrates symmetric bilateral severe atrophy involving the caudate nuclei, putamen, and globus pallidi bilaterally with consequent enlargement of the frontal horns of the lateral ventricles (*arrows*). There is also diffuse prominence of the sulci indicating generalized cortical atrophy. Axial (***B***) and coronal (***C***) FLAIR images demonstrate bilateral symmetric abnormal high signal in the caudate and putamen.
Coronal T1-weighted image (***D***) demonstrates enlarged frontal horns with abnormal configuration. Also note diffusely decreased marrow signal, which could represent anemia or myeloproliferative disease.

Copyright © 2008 The McGraw-Hill Companies. All rights reserved.

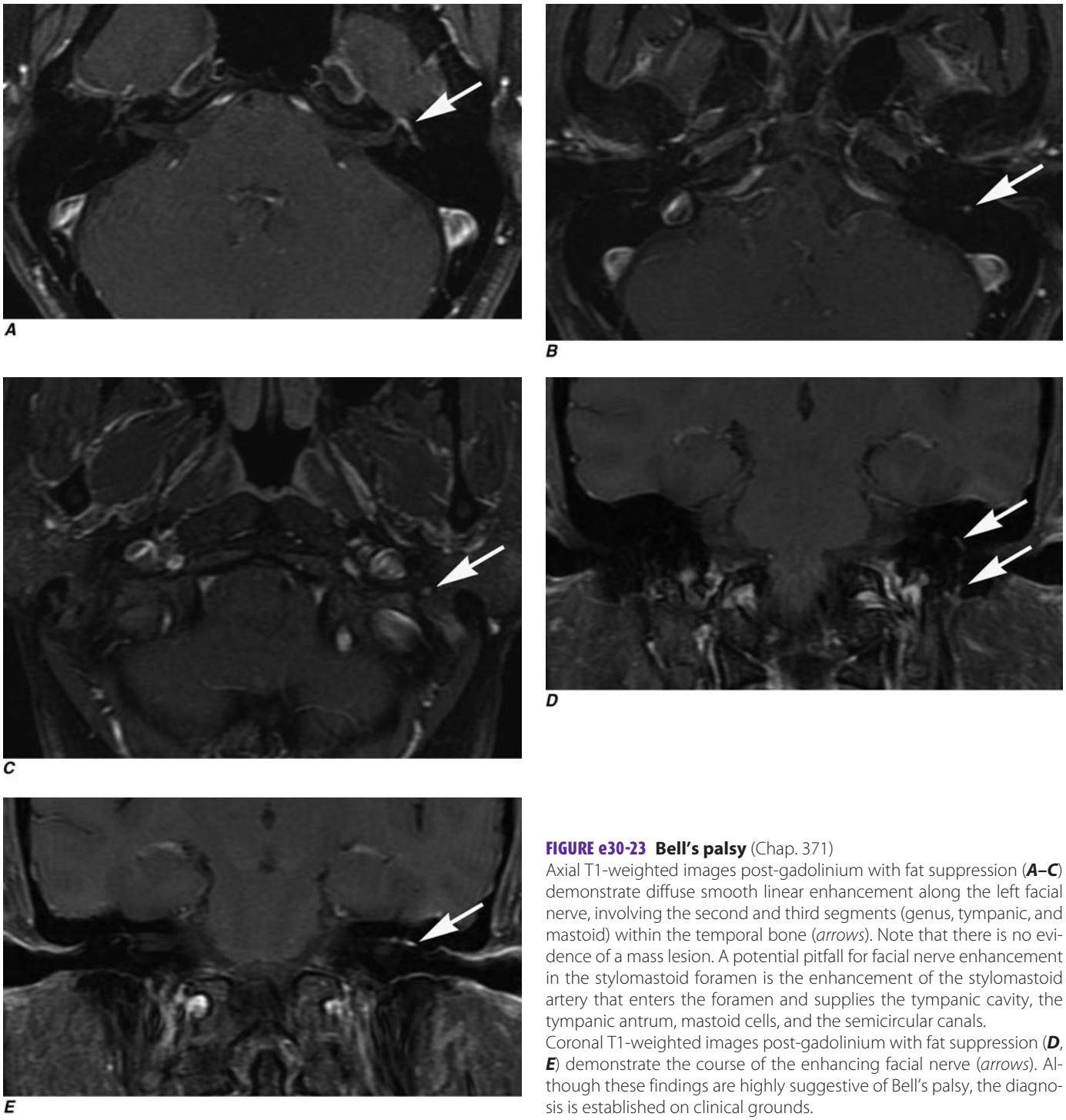

FIGURE e30-23 Bell's palsy (Chap. 371)
Axial T1-weighted images post-gadolinium with fat suppression (***A–C***) demonstrate diffuse smooth linear enhancement along the left facial nerve, involving the second and third segments (genus, tympanic, and mastoid) within the temporal bone (*arrows*). Note that there is no evidence of a mass lesion. A potential pitfall for facial nerve enhancement in the stylomastoid foramen is the enhancement of the stylomastoid artery that enters the foramen and supplies the tympanic cavity, the tympanic antrum, mastoid cells, and the semicircular canals.
Coronal T1-weighted images post-gadolinium with fat suppression (***D***, ***E***) demonstrate the course of the enhancing facial nerve (*arrows*). Although these findings are highly suggestive of Bell's palsy, the diagnosis is established on clinical grounds.

Copyright © 2008 The McGraw-Hill Companies. All rights reserved.

FIGURE e30-24 Spinal cord infarction (Chap. 372)
Sagittal T2-weighted MR image of the lumbar spine (***A***) demonstrates poorly defined areas of abnormal high signal in the conus medullaris and mild cord expansion (*arrow*).
T1-weighted MR image of the lumbar spine post-gadolinium (***B***) demonstrates mild enhancement (*arrow*).
Sagittal diffusion-weighted MR image of the lumbar spine (***C***) demonstrates restricted diffusion (*arrow*) in the areas of abnormal high signal on the T2-weighted image (***A***).

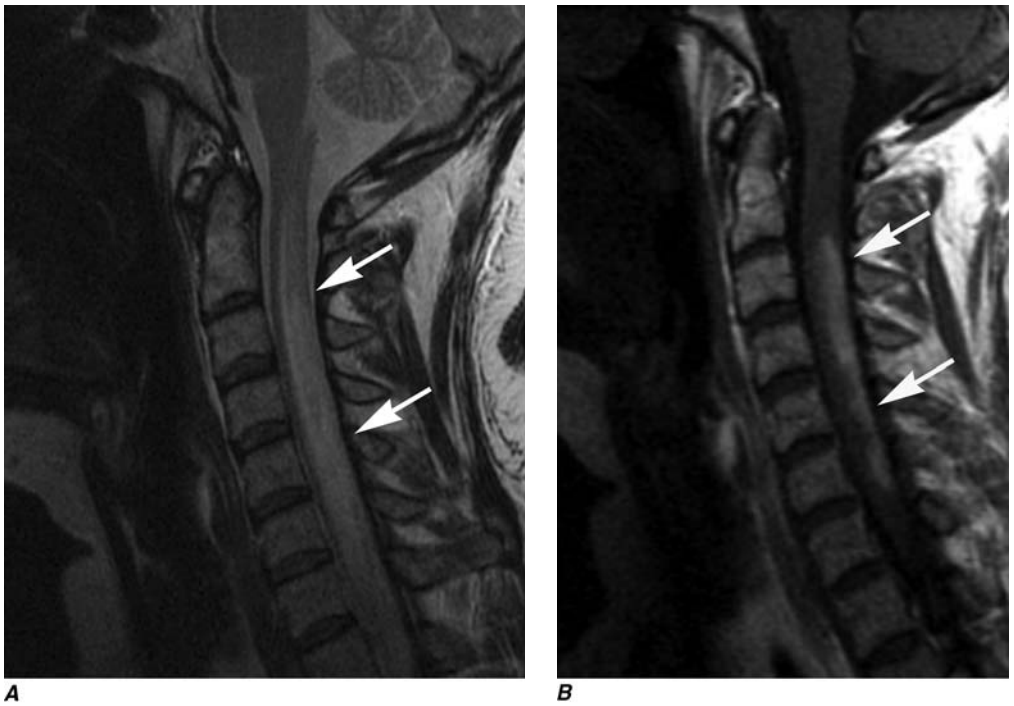

FIGURE e30-25 Acute transverse myelitis (Chap. 372)
Sagittal T2-weighted MR image (***A***) demonstrates abnormal high signal in the cervical cord extending from C1 to T1 with associated cord expansion (*arrows*).
Sagittal T1-weighted MR image post-gadolinium (***B***) demonstrates abnormal enhancement in the posterior half of the cord from C2 to T1 (*arrows*).

Copyright © 2008 The McGraw-Hill Companies. All rights reserved.

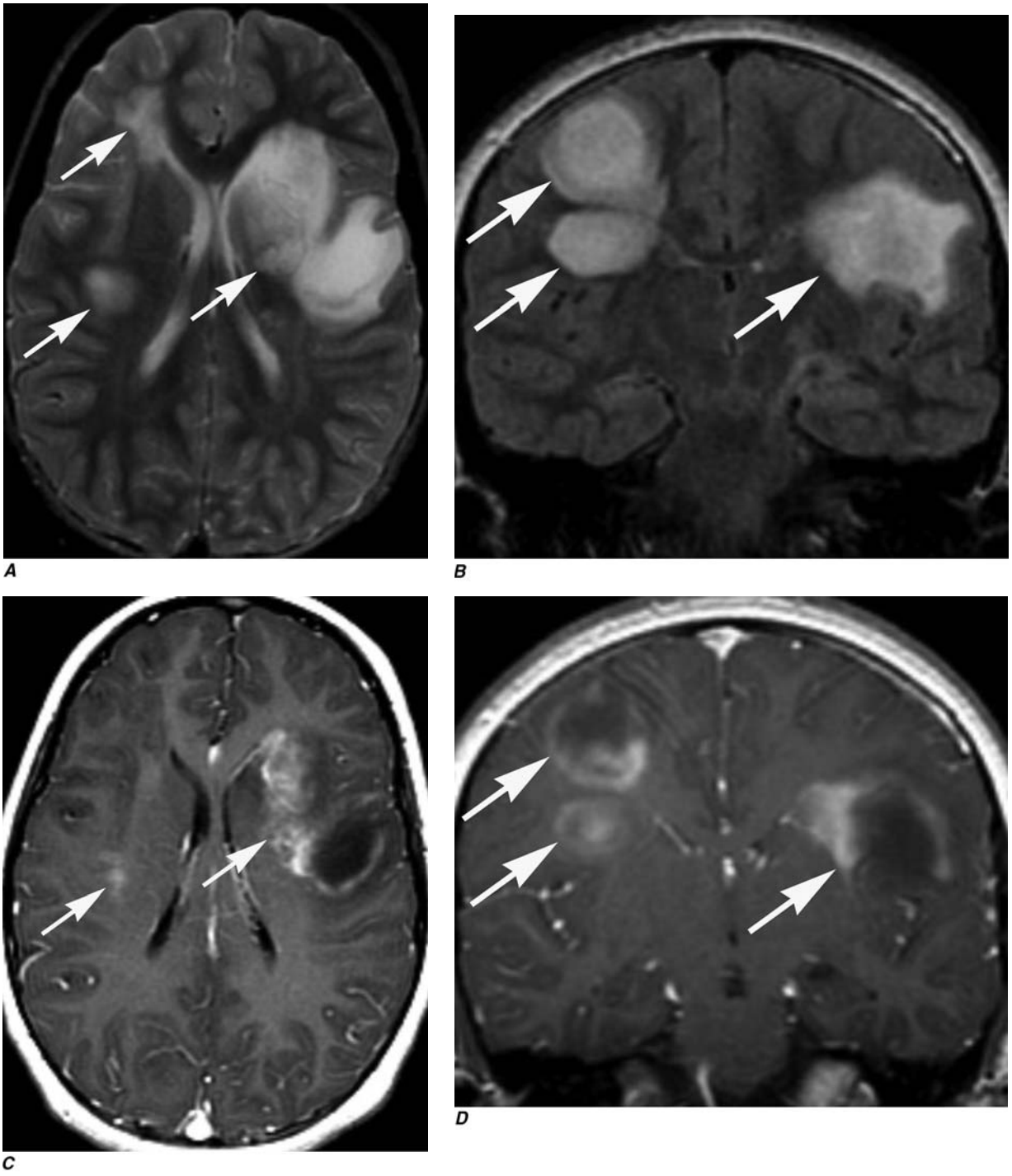

FIGURE e30-26 Acute disseminated encephalomyelitis (ADEM) (Chap. 375)
Axial T2-weighted (***A***) and coronal FLAIR (***B***) images demonstrate abnormal areas of high signal involving predominantly the subcortical white matter of the frontal lobe bilaterally, and left caudate head. Following administration of gadolinium, corresponding axial (***C***) and coronal (***D***) T1-weighted images demonstrate irregular enhancement consistent with blood-brain barrier breakdown and inflammation; some lesions show incomplete rim enhancement, typical for demyelination.

Copyright © 2008 The McGraw-Hill Companies. All rights reserved.

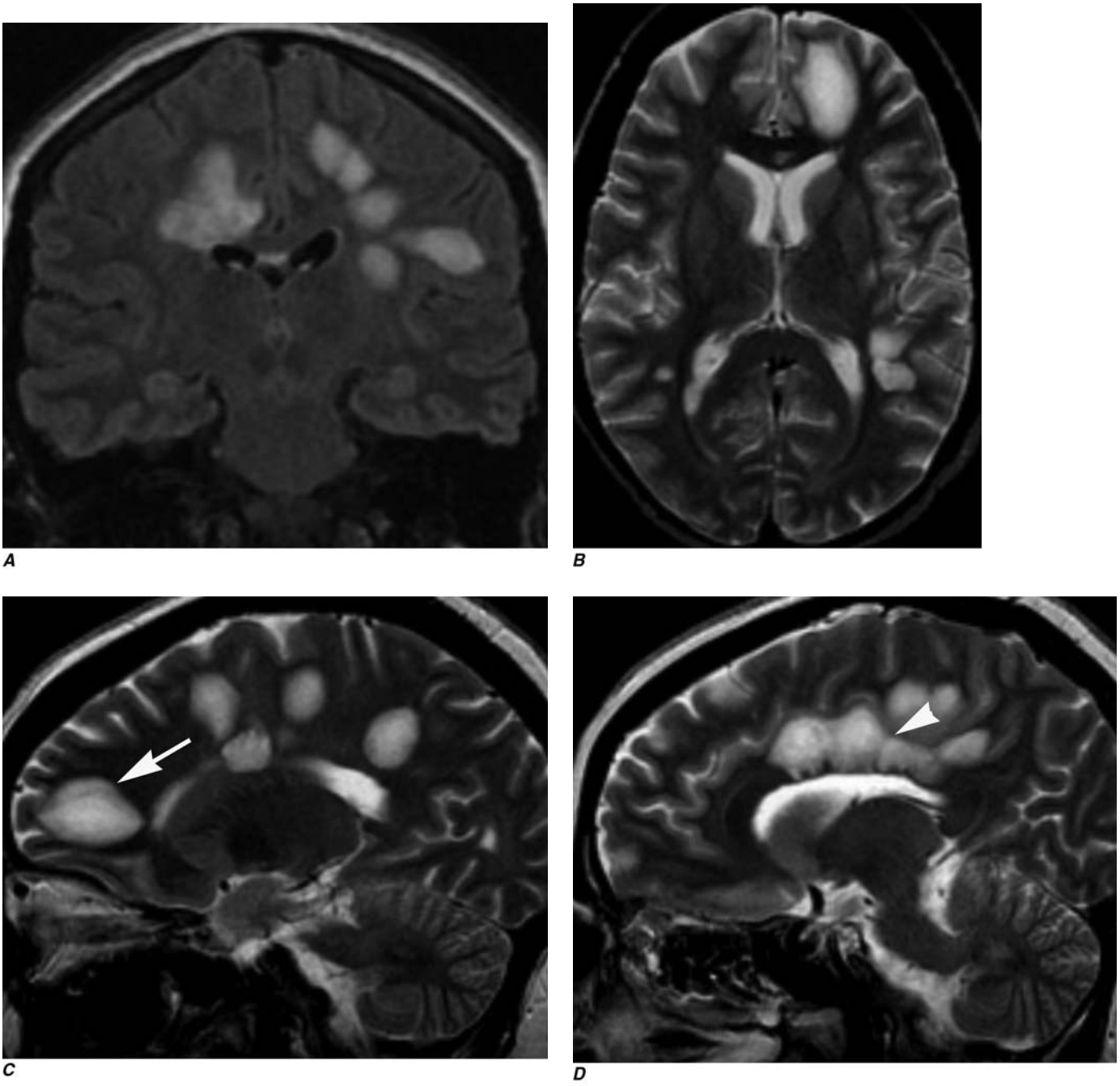

FIGURE e30-27 Balo's concentric sclerosis (a variant of multiple sclerosis) (Chap. 375)
Coronal FLAIR MRI (***A***) demonstrates multiple areas of abnormal high signal in the supratentorial white matter bilaterally. The lesions are ovoid in shape, perpendicular to the orientation of the lateral ventricles, and with little mass effect. Axial (***B***) and sagittal (***C–E***) T2-weighted MR images demonstrate multiple areas of abnormal high signal in the supratentorial white matter bilaterally, as well as the involvement of the body and splenium of the corpus callosum and the callosal-septal interface (*arrowhead*). Some of the lesions reveal concentric layers, typical of Balo's concentric sclerosis (*arrows*). *(continued)*

Copyright © 2008 The McGraw-Hill Companies. All rights reserved.

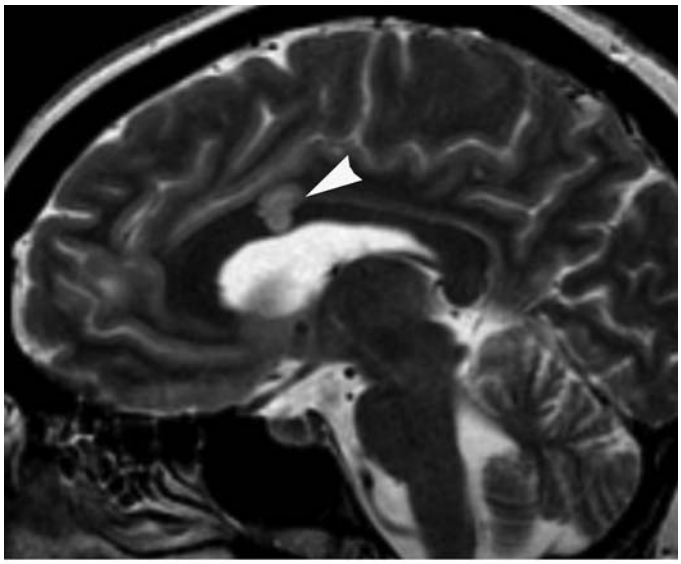

E

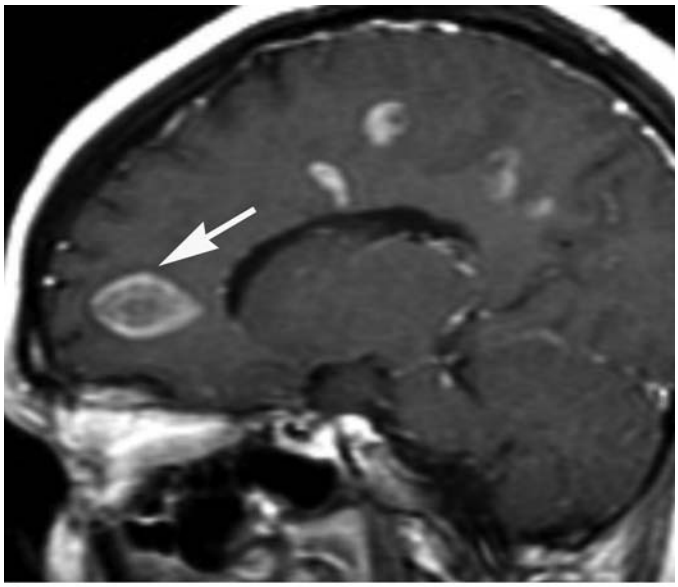

F

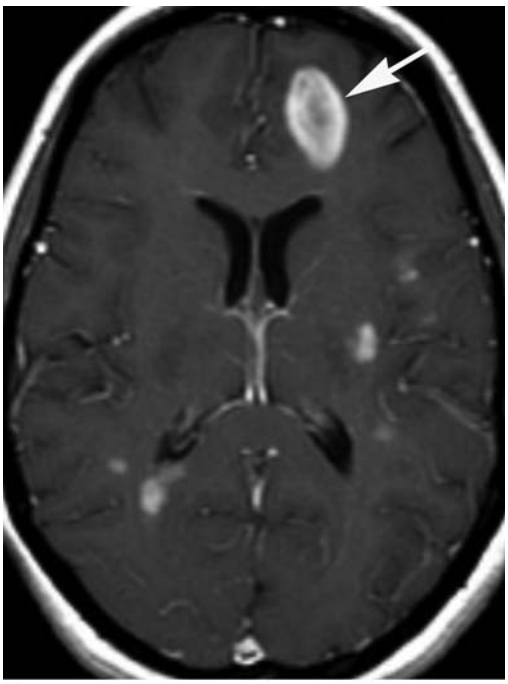

G

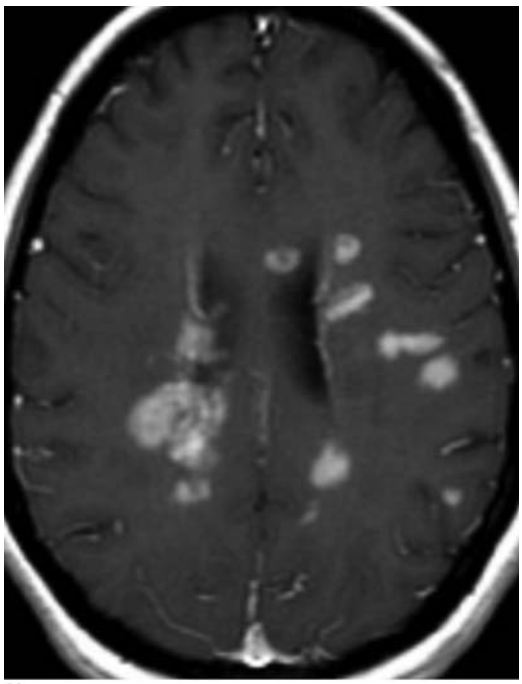

H

FIGURE e30-27 (*Continued*)
Sagittal (***F***) and axial (***G***, ***H***) T1-weighted MR images post-gadolinium demonstrate abnormal enhancement of all lesions with some of the lesions demonstrating concentric ring enhancement (*arrows*).

Copyright © 2008 The McGraw-Hill Companies. All rights reserved.

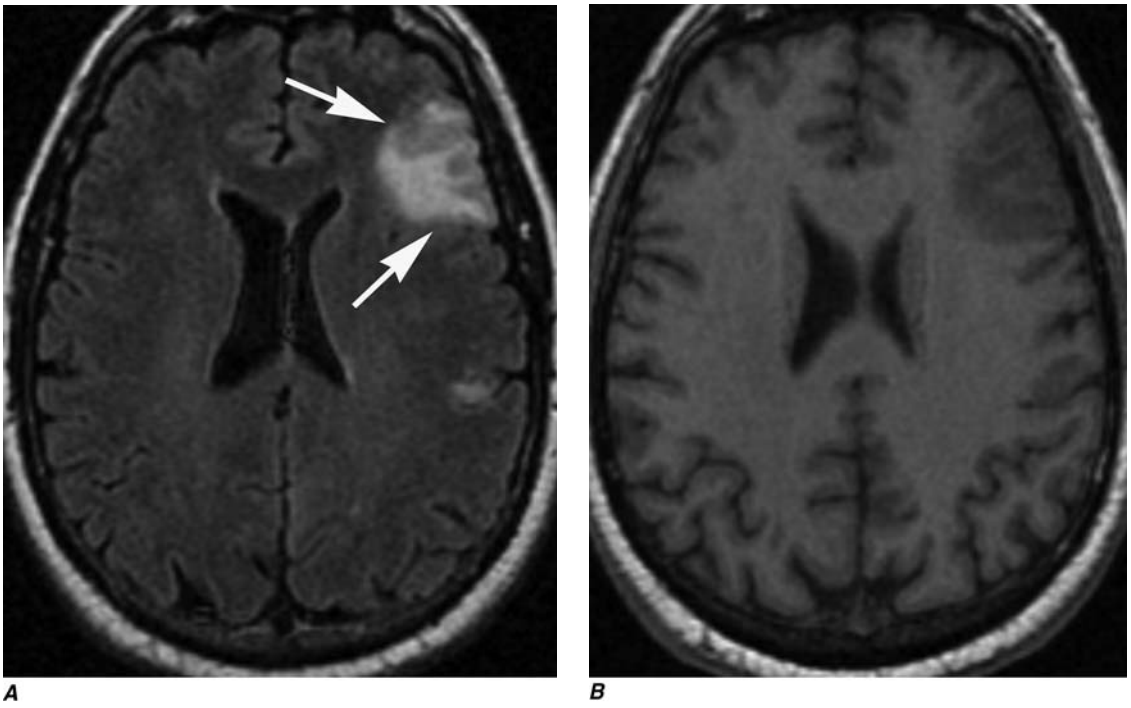

FIGURE e30-28 Hashimoto's encephalopathy (Chap. 376)
Axial FLAIR (***A***) demonstrates focal area of abnormal high signal involving the gray and white matter in the left frontal lobe. There is also a small area of abnormal high signal in the precentral gyrus.
Axial T1-weighted images (***B***, ***C***) pre- and post-gadolinium demonstrate cortical/pial enhancement in the region of high signal on FLAIR.

Copyright © 2008 The McGraw-Hill Companies. All rights reserved.

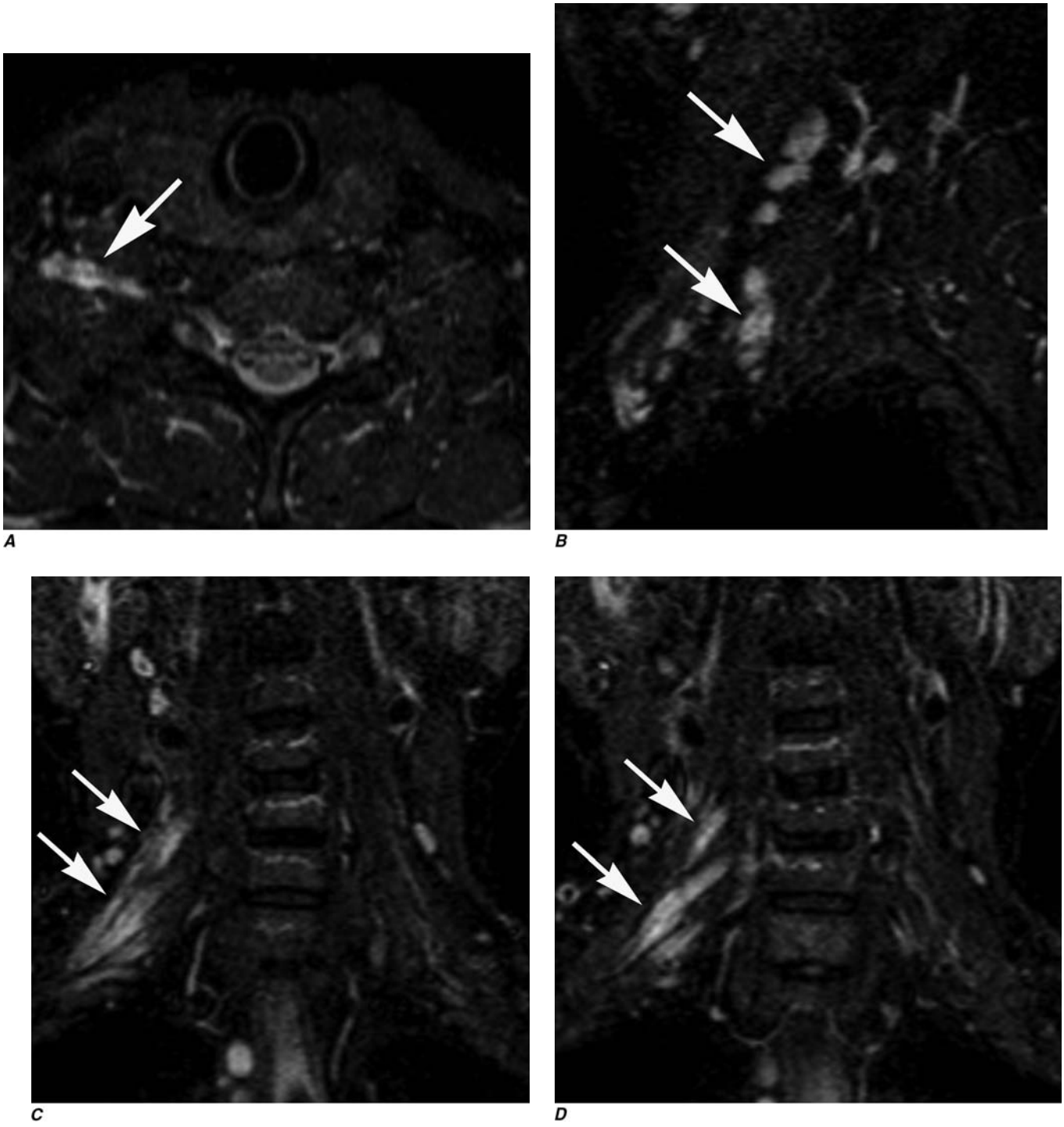

FIGURE e30-29 Brachial plexopathy (Chap. 379)
Axial (***A***), sagittal (***B***), and coronal (***C***, ***D***) short tau inversion recovery (STIR) MR images demonstrate abnormal enlargement and abnormal high signal involving the right C6, C7, and C8 nerve roots, and the trunks and divisions that originate from these roots *(arrows)*. *(continued)*

Copyright © 2008 The McGraw-Hill Companies. All rights reserved.

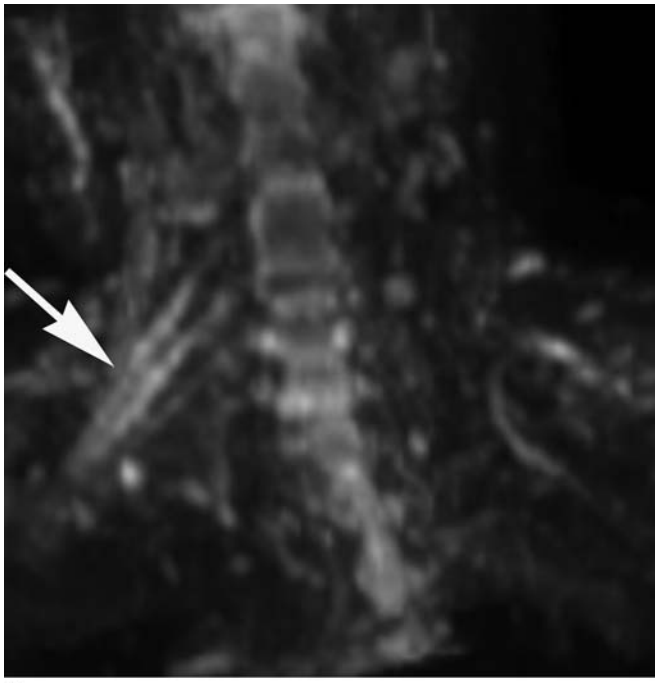

E

FIGURE e30-29 (*Continued*)
Diffusion-weighted MR imaging (***E***) demonstrates abnormal reduced diffusion within the right C6, C7, C8 nerve roots and their corresponding trunks and divisions (*arrow*). These findings are compatible with radiation-induced brachial plexopathy.

Copyright © 2008 The McGraw-Hill Companies. All rights reserved.